This project has received funding from the Euratom research and training programme 2014-2018 under grant agreement No 662287.

EJP-CONCERT

European Joint Programme for the Integration of Radiation Protection Research

H2020 – 662287

D9.129 – Final Project Report

Lead Author: ENEA

Reviewer(s): Soile Tapio, Munira Kadhim, Fiona Lyng

and CONCERT coordination team

Work package / Task	**WP9 Task9.7 SEPARATE**	
Deliverable nature:	**Report**	
Dissemination level: (Confidentiality)	**Public**	
Contractual delivery date:	**Month 56**	
Actual delivery date:	**Month 56**	
Version:	**1**	
Total number of pages:	**33**	
Keywords:	**Whole-body irradiation (WBI); Partial-body irradiation (PBI); dosimetry; proteomics; raman spectral analysis; miRNomes analysis, bioinformatics; hippocampus; neurogenesis; heart; liver, exosome**	
Approved by the coordinator:	**M56**	
Submitted to EC by the coordinator:	**M56**	

Table of Content

Abstract

Radiation effects are not confined to directly irradiated tissues. Living organisms cope with injury through coordinated cell/tissue responses, therefore, *in vivo* data on out-of-target responses can be very powerful because of the physiologic cellular connections within a tissue or cross-talk among tissues. Partial body exposures are the norm rather than the exception in many fields in which radiations are involved. The contribution of systemic "out-of-target" effects to the risks of long term detriment following exposure to radiation is largely unknown. Indeed, both protective and damaging effects have been described. From the radiation protection viewpoint this level of uncertainty of the risk is problematic, as workplace, environmental and medical exposures frequently involve partial body exposure. Nevertheless, there is a general lack of *in vivo* data for the radiation out-of-target effects relevant for human exposures and only limited data are available that allow understanding of their generality in tissues/systems *in vivo* and underlying mechanistic bases. In particular, these effects have not been adequately investigated in the context of brain exposure (i.e. cancer and cognitive risks), heart exposure (i.e. cardiovascular risks), or liver exposure (i.e. cancer and metabolic alteration risks).

The SEPARATE project aimed to determine the differences/similarities between in-field and out-of-field responses in normal tissues. The consortium - internationally recognized for its large experience in radiation biology, animal studies, molecular biology, bioinformatics, physics and metabolomics – includes three different European partners (ENEA, Italy; HMGU, Germany; OBU, UK) and one third party (TU, Ireland), each one at the forefront of their respective fields in radiation biology. The changes in the transcriptome (coding and non-coding), proteome and metabolome have been explored, in out-of-target and directly irradiated tissues vs. unexposed control. By integrative bioinformatics analysis, we compared molecular pathways affected in in-field and out-of-field organs. We also examined the role of exosomes as possible mediators of radio-induced damage signals and, after extracting them from tissues and blood of exposed and unexposed mice, we extensively characterized their size, concentration and cargo. Results clearly indicate that the out-of-field organs exhibit molecular changes nearly identical to those found in directly irradiated organs and that exosomes are able to propagate radiation signaling by modifying viability and level of DNA damage in recipient Mouse Embrionic Fibroblasts (MEF) cells *in vitro*. These findings, besides improving the current understanding of the contribution of systemic "out of target" effects caused by exosome-mediated radiation signaling, that might have potentially important implications in the clinic and impact the risks of long-term health detriment by radiation.

Project structure

The SEPARATE project was organized into 5 WPs: WP1: Partial body irradiation and Dosimetry; WP2: Omics analyses and biomarkers; WP3: Radiation signaling between tissues; WP4: Project management; WP5: Dissemination, training, exploitation.

Activities in WP1 were devoted to setting up PBI and to establishing experimental measurements to ensure that the out-of-field effects under study were not the result of photons crossing the lead shield or deflected in the cap through the irradiated tissues. Using two independent methodologies (i.e. first a NE 2571 ionization chamber inserted in the same position as the brain, heart and liver and successively gafchromic films) the attenuated and scattered dose was measured and considered not significant in our experimental conditions. A total of 200 C57BL/6J mice (160 irradiated + 40 controls) were enrolled in the study of out-of-target radiation effects on shielded hippocampus, cortex, liver and heart, after doses of 0.1 or 2 Gy of X rays to the lower third of the body. Mouse groups were sacrificed 15 days or 6 months post-irradiation, and tissues/organs collected and distributed to partners. It was also established that the ultracentrifugation method resulted in the highest yield of exosomes therefore, it was adopted for extraction from tissues of control, irradiated (WBI) and shielded mice (PBI). Within WP2, changes at the transcriptome, non-coding RNAs, protein and metabolic levels were evaluated in out-of-field organs known to be impaired by direct ionizing radiation exposures. To this aim, methodologies based on NGS, PCR arrays, proteomics and Raman spectroscopy have been adopted. In WP3, investigations on exosomes from exposed and shielded tissues and from blood, and their specific bioactive cargo, were carried out to establish their role in mediating out-of-target effects. In vitro, different biological endpoints were analyzed after treatment of mouse embryonic fibroblasts (MEFs) with exosomes obtained from organs of CN, TBI and PBI mice. In vivo, different intracranial injections were tested to demonstrate exosomes-mediated DNA damage.

WP1 – Partial-body irradiation and Dosimetry WP Leader ENEA

Work performed within WP1 of SEPARATE was focused on the partial- and whole-body-irradiation of C57Bl/6 female mice of 80 days of age with 0.1 or 2Gy of x-rays (Fig.1). This work has been completed as well as transfer of experimental material to project partners. A detailed description of dosimetry and procedure is provided in Deliverables D9.122 (Irradiation and dosimetry procedures) and D9.123 (Completion of PBI/WBI). Under WP1, in order to optimize the exosome isolation methods from mouse organs, pilot experiments with three different methods of exosome's isolation and analysis: i) ultracentrifugation, ii) chemical/EV column, and iii) Viva Spin Column, were conducted. The ultracentrifugation method resulted in the highest yield of exosomes for the brain (Fig. 2) and was therefore adopted. Characterization of exosomes from irradiated and shielded tissues have been described in Deliverable D9.124.

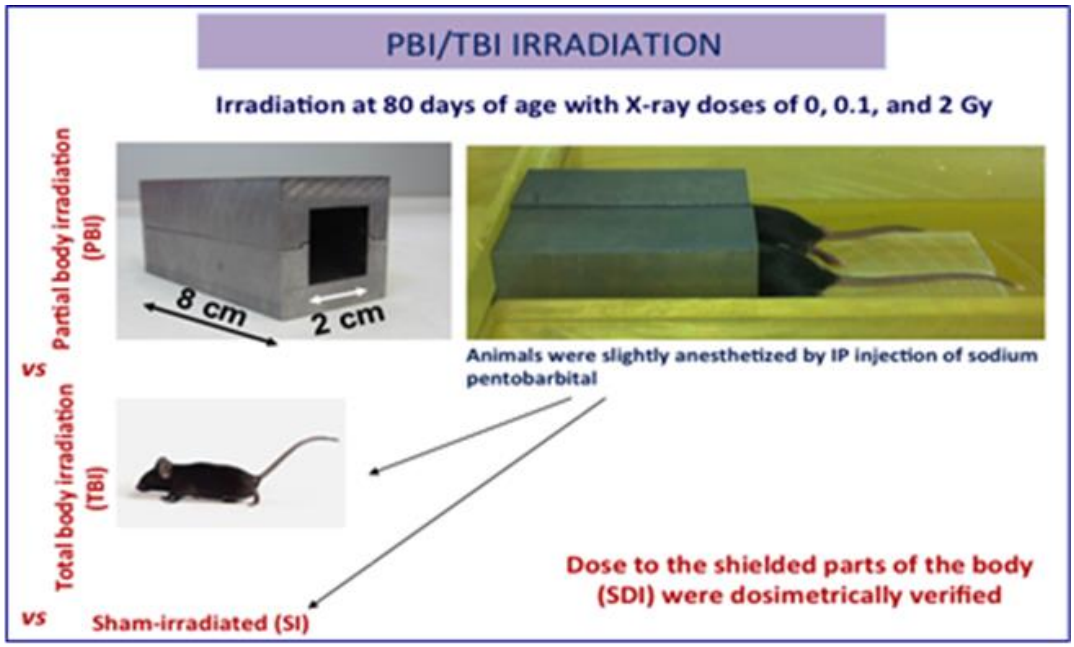

Fig. 1. Irradiation modalities

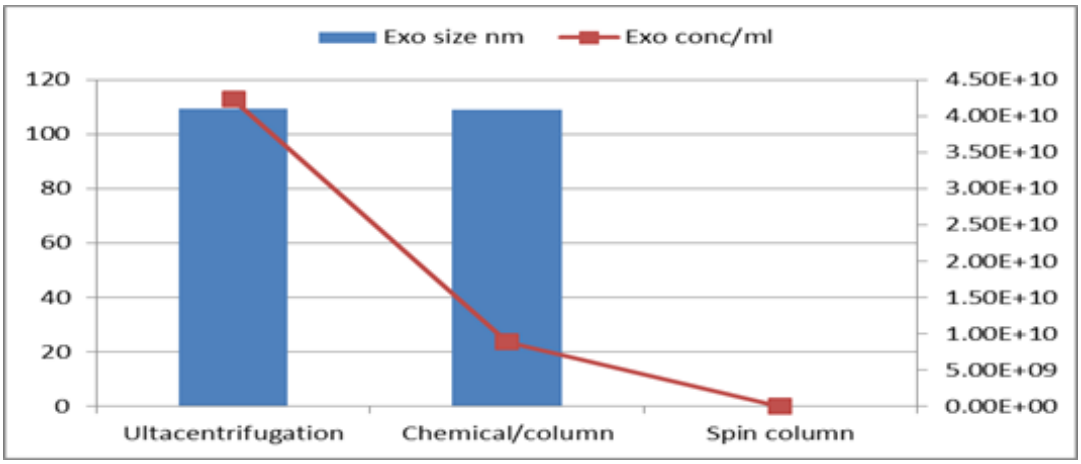

Fig. 2: Mouse brain. Data from the three different methods of exosome extraction.

WP2 - Omics analyses and Biomarkers – WP Leader HMGU

WP2 focused on the analyses of the changes at the transcriptome, non-coding RNAs, protein and metabolic levels on out-of-field organs known to be impaired by direct ionizing radiation exposure following exposure of the lower third of the body, whilst the target organs are shielded. WP2 describes progress to date in the molecular studies focused on establishing the role of proteomic and metabolic changes in "out-of-target" effects in hippocampus and heart through "omics" analyses based on performed at ENEA, HMGU and TU Dublin. All the analyses have been performed at 2 weeks and 6 months post-irradiation.

By means of omics analyses, an important goal achieved within the project was the demonstration that in-field and out-of-field irradiation cause nearly identical modification in non-coding RNAs, proteome and metabolome at 15 days post-irradiation, especially after irradiation with 2 Gy. Through miRNome analysis based on NGS, we observed changes in miRNAs in out-of-field hippocampus and heart 15 days after PBI with 2 Gy of X-rays that were also detected in corresponding tissue of whole body irradiated (WBI) mice. MiRNome analysis also revealed that, compared to the heart, the hippocampus shows a higher level of deregulated miRNAs in common between in-field and out-of-field tissues, suggesting a peculiar sensitivity to radiation-induced abscopal effects; noteworthy, many of these perturbed miRNAs and predicted target pathways are known to be involved in brain and heart pathology (Fig. 3). However, over 54% of the deregulated miRNAs were in common between out-of-field hippocampus and heart, suggesting that PBI, through a miRNA-mediated common molecular mechanism, has the potential to induce specific tissue-dependent reactions in shielded tissue. We also investigated whether after irradiation with a low dose (0.1 Gy) miRNAs found differentially expressed in PBI and WBI hippocampi at 2 Gy were still perturbed. Quantitative expression of the subset of miRNAs (n=25) was evaluated by qRT-PCR custom plates. The analysis revealed only 3 differentially expressed miRNAs in WBI hippocampi (miR-143-5p, miR-378a-3p, miR-378a-5p; p-value = 0.04) and no statistically significant deregulation after PBI, suggesting a dose-dependent perturbation of miRNAs both in in-field and out-of-field hippocampus. A detailed description of data set on NGS-based mirNome analysis in irradiated and shielded tissues is provided in deliverable D9.127.

Fig. 3. (**A**) Venn diagram of the significantly deregulated miRNAs (|log2FC| > 3 and p-value of < 0.1) shared in the

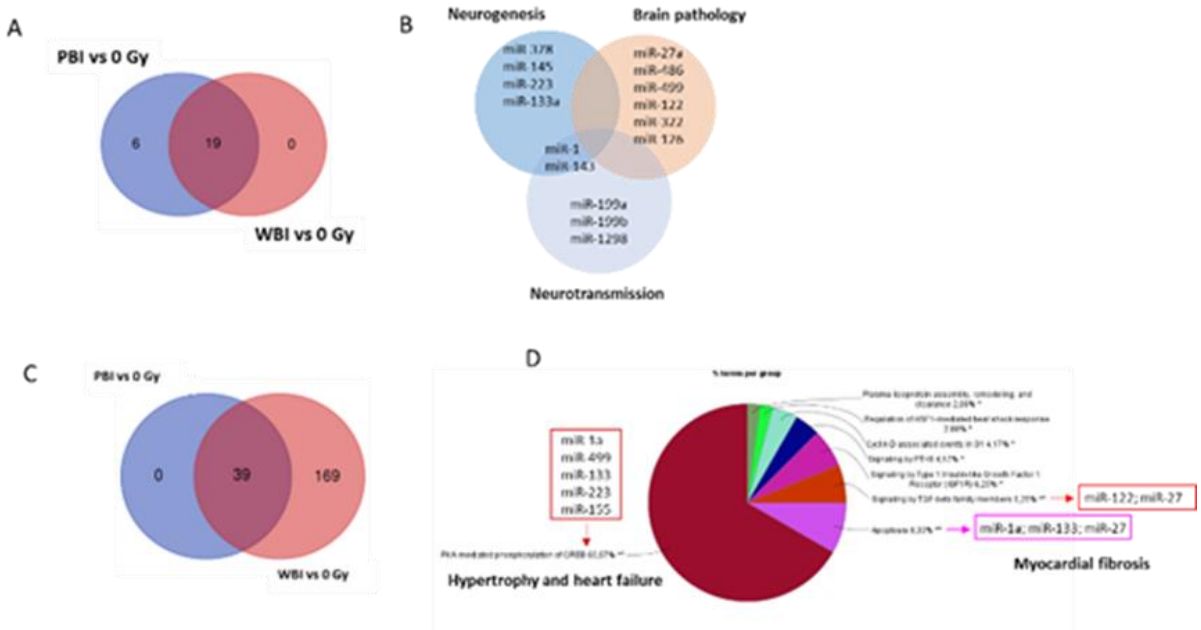

hippocampus of PBI and WBI mice vs. CN mice. (**B**) miRNAs known to be involved in brain-related functions. (**C**) Venn diagram of the significantly deregulated and shared miRNAs in the heart of PBI and WBI mice vs. CN mice and (D) pathway analysis predicted by the significantly altered miRNAs in common after PBI or WBI.

Similarly, proteomic profiles indicated that a high percentage of the significantly deregulated proteins in PBI hippocampi overlapped with those altered following WBI both in 0.1 Gy (49%, 46/94) and 2 Gy (80%, 89/111) groups at 15 days and 6 months postirradiation (53% at 0.1 Gy, 18/34; 56% at 2 Gy, 44/79). Both direct and abscopal effects alter biological pathways that are associated with learning and memory, suggesting that WBI and PBI cause very similar alterations in the proteome. Together with metabolomics analysis both WBI and PBI (2.0 Gy) induce partly similar effects 2 weeks after the irradiation in the hippocampus (Fig. 4). At the proteomic level, this overlap disappears almost completely at the 0.1 Gy dose with time (6 months) and largely also with the 2 Gy dose. In contrast to hippocampus, the heart shows no similarities between WBI and PBI at the metabolic level (2 weeks and 6 months), although the proteomic and metabolomic response of both WBI and PBI clearly differs from the sham-irradiated control. Taken together, both the hippocampus and the heart show the induction of marked alterations after PBI, especially 2 weeks after irradiation, but while in the hippocampus proteomic and metabolomic alterations induced by PBI were similar to those induced by WBI, they largely differed in the heart. Data set on proteomic and metabolic changes in irradiated and shielded tissues is presented in deliverable D9.126.

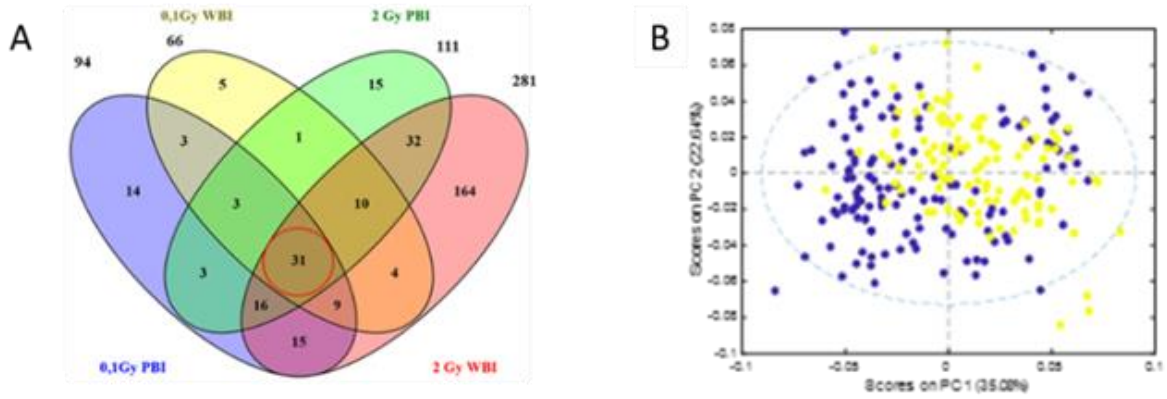

Fig. 4. (**A**) The Venn diagram shows the number of significantly deregulated and shared proteins in irradiated hippocampus 15 days after exposure to 0.1 or 2.0 Gy in WBI or PBI set up. (**B**) Principal Component Analysis (PCA) scatter plot of 2 Gy WBI and 2 Gy PBI groups.

Since the omics indicated that out-of-field hippocampus from PBI mice displays changes in multi-omic profiles similar to those caused by WBI, we thought to investigate whether PBI may also cause phenotypically detectable alteration in the cellular composition of the dentate gyrus. Neurogenesis—the generation of new neurons—is an ongoing process that persists in the adult mammalian brain of several species, including humans. Impairment of hippocampal neurogenesis is frequently observed after whole-brain exposure, and it is regarded as the most important mechanism of radiation-induced cognitive dysfunction. Through a methodology based on a combination of morphological cellular features and immunohistochemistry with stage-specific neurogenesis markers, we have investigated the dysfunction in the SGZ of the DG (Fig. 5A). The radial glia-like stem cells (G-FAP) maintain their pool through self-renewal and give rise to progenitor cells with different morphology (Sox2), which undergo rapid proliferation (Ki-67) and begin to express markers specific to the neuronal fate becoming newborn neurons (DCX).

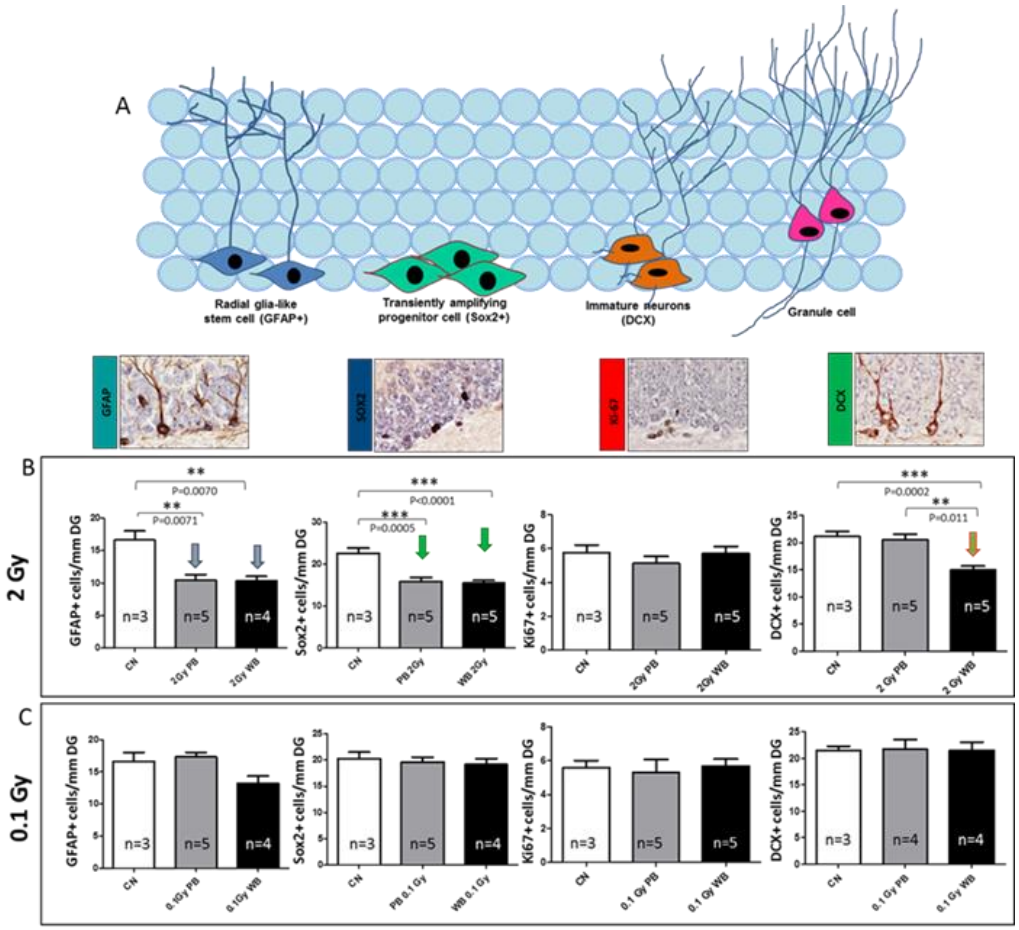

Fig. 5: Effect of in-field or out-of-field X-rays irradiation on adult hippocampal neurogenesis at 15 days post-irradiation. (**A**) Developmental stages in the course of adult hippocampal neurogenesis **(B)** effect at 2 Gy **(C)** effect at 0.1 Gy**.**

We detected a significant reduction of 37.22% in the number of NSCs labelled by GFAP in PBI compared to unexposed DG (p = 0.0071) (p = 0.0070) and a similar significant decrease of 37.70 in WBI (Figure 5B). In addition, compared to unexposed hippocampus we also observed significant reduction in the percentage of neural stem cell precursors labelled by Sox2 of 19.56% (p = 0.0476) and 25.62% (p = 0.0074) in PBI and WBI respectively. Instead, no changes in the number of proliferating cells labelled by Ki-67+ were detected in PBI and WBI compared to unexposed mice. Finally we observed a significant reduction of 32.77% (p = 0.046) in immature neurons labelled by DCX in the DG of WBI mice but not in PBI mice, representing the unique difference in the defects induced by the two exposure modalities. Altogether our findings clearly demonstrated that *"*out-of-field" irradiation causes defects in the dynamic transition among neural stages in the DG nearly identical to those induced by in field irradiation. These defects, including self-renewal and proliferation, point to a complex disturbance in the control of progression of NSCs into neurons in the hippocampus by out-of-field irradiation. However while for WBI these defects (i.e. significant depletion of cells labelled by GFAP, Sox2 and DCX) persisted at 6 months post-irradiation, for PBI their were transient and were fully recovered at 6 months post-irradiation (data not shown).

To investigate whether low dose exposure induces perturbation of hippocampal neurogenesis we have evaluated the radiation-dependent modifications in the cellular composition of the SGZ of the DG 15 days post-irradiation with 0.1 Gy of X-rays in WBI or PBI mice. Compared to unirradiated mice, no significant changes were detected in any of the DG cellular population (GFAP; Sox2, Ki-67 and DCX) in WBI and PBI mice (Fig. 5 C). Altogether, molecular and cellular findings presented provide a robust proof of principle of out-of-target radiation responses in the hippocampus in vivo.

WP3 - Radiation signalling between tissues - WP Leader OBU

In WP3, exosomes from exposed and shielded ortgans blood plasma, were investigated for their specific bioactive cargo, in order to establish their role in mediating out-of-target effects. In vitro, different biological endpoints were analyzed after treatment of MEF cells with exosomes obtained from organs of WBI and PBI mice. In vivo, different intracranial injections were tested to demonstrate exosomes-mediated DNA damage.

Task 3.1 To characterize exosomes (OBU, HMGU, TU)

In this task, we characterized the exosomes derived from WBI and PBI organs (liver, heart and brain) and plasma. Taken together these results show that ionising radiation can increase the yield of exosomes derived from mouse organs 24 hours and 15 days after irradiation. Differences in the mean diameter of exosomes are statistically not significant for both time points, indicating that ionising radiation does not alter the size distribution of exosomes.

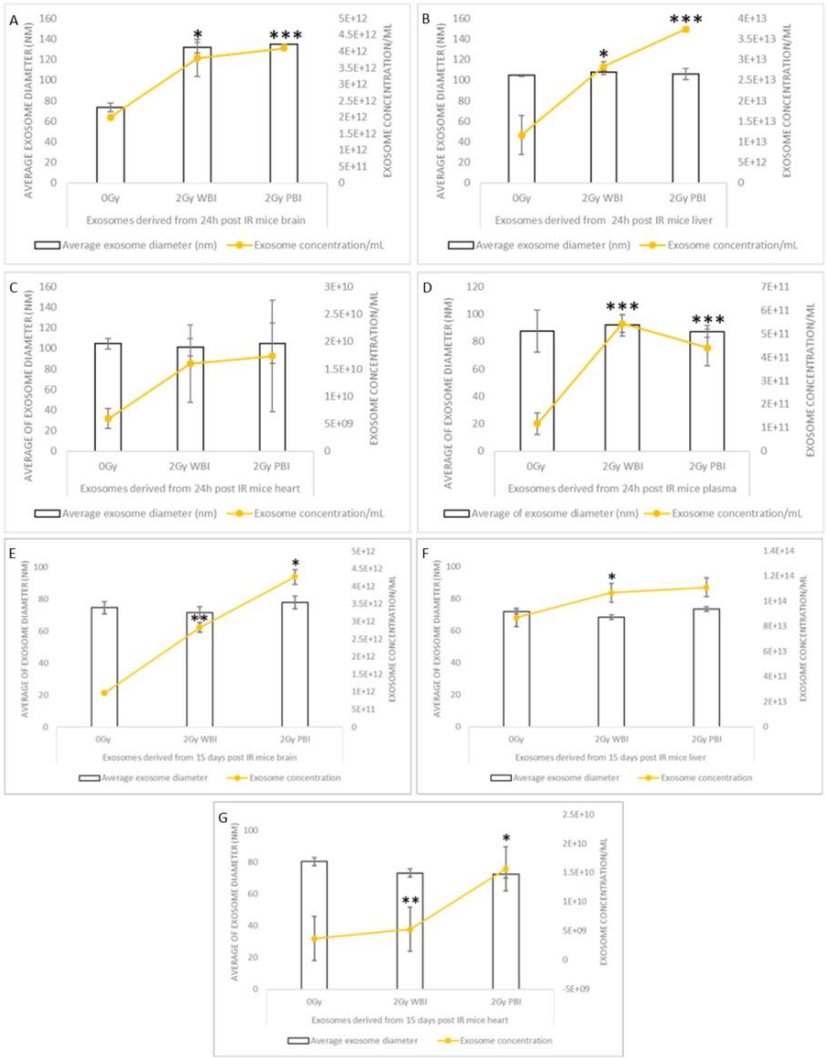

Fig. 6. Concentration (exosome/ml) and size (nm) distribution of exosome suspensions obtained from 24 hours post IR (**A-D**) and 15 days post IR (**E-G**) 2Gy WBI and 2Gy PBI mice organs (brain, liver, heart) and plasma compared to unirradiated conterparts. Bars represent mean ± SD; significance was tested by Student's t-test (*p < 0.05, **p < 0.01, ***p < 0.001).

Exosomes characterization, their *in vitro* and *in vivo* functional testing, as well as their miRNA and protein cargo are being analysed and extensively described in WP3 section of this document.

Furthermore, presence of exosome was confirmed by Western blot analysis against the exosome marker CD63 (Fig. 7A). Exosome size, evaluated by transmission electron microscopy (TEM), resulted between 70-120 nm in diameter (Fig. 7B).

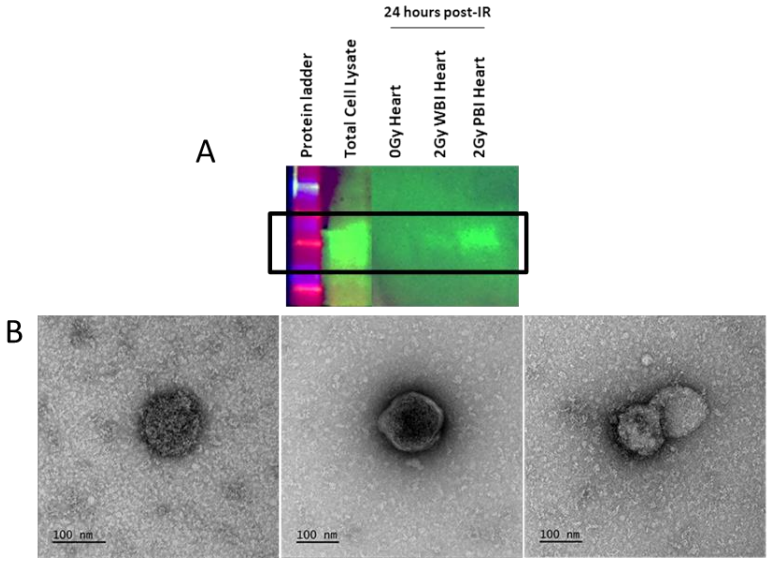

Fig. 7. Exosome characterization (**A**) Western blot analysis of exosomes for CD63, TSG101 and GM130. Lane 1 protein ladder, lane 2: total cell lysate, lane 3: unirradiated (0Gy) heart sample, lane 4: 2Gy WBI heart protein and lane 5: 2 Gy PBI heart protein sample. (**B**)TEM representative images of 1:10 diluted plasma exosome samples.

3.1.1 Radiation-induced changes in exosome cargo in PBI and WBI plasma and organs

Here we investigated the cargo of exosomes collected from plasma at 24 hours after WBI and PBI irradiation and from whole brain, heart, and liver at 24 hours or 15 days after WBI and PBI irradiation. For proteomic methods refer to Deliverable D 9.1262 and for NGS-based miRNome analysis to D9.127.

NGS-based miRNome analysis of the plasma exosomes 24 hours after PBI or WBI

To test miRNA involvement in out-of-field effects we compared the perturbation induced by in-field and out-of-field X-ray irradiation in the miRNA cargo of exosomes extracted from plasma. Here we reported a first characterization of the radiation-induced changes in the miRNA cargo of exosome isolated from plasma of 2Gy-WBI and 2Gy-PBI mice (Fig. 8A and 8B). The Venn diagram (Fig. 8C) shows that 57 miRNAs were significantly modulated after WBI and only 13 after PBI; all the deregulated miRNAs were upregulated. These findings might suggest that the amount of radiation exposed tissues strongly influences the miRNA cargo of exosomes released. Differently from the nearly complete overlap in deregulated miRNAs between WBI and PBI in the hippocampus at 15 days postirradiation, only 5 miRNAswere commonly upregulated between WBI and PBI plasma exosomes; the list is shown in Fig. 30C. Further analysis in this catalogue of miRNAs modulated in response to radiation exposure will be necessary to understand their possible role in mediating out-of-field effects.

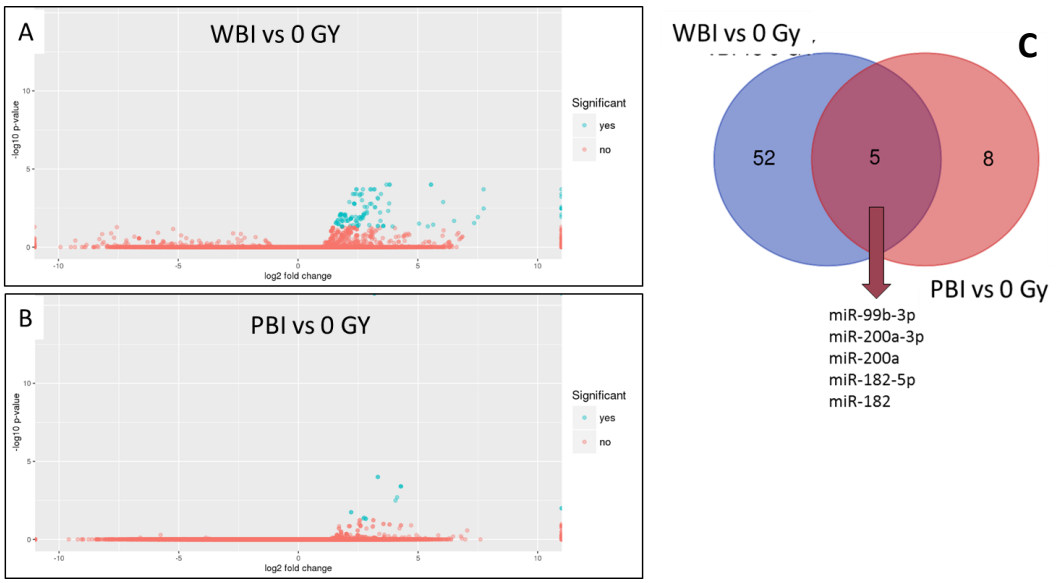

Fig. 8. Volcano plots showing fold-change and p-values of all differentially expressed miRNAs between WBI-irradiated (2 Gy) plasma exosomes vs 0 Gy (**A**) and PBI-irradiated (2 Gy) plasma exosomes vs. 0 Gy (**B**). Fold-change (log2) versus significance (-log10 p-value) for each miRNA is shown. Significant miRNAs (FDR < 0.05) are in blue. (**C**) Venn diagrams showing the number of significantly deregulated and shared proteins in exosomes isolated from plasma at 24h after exposure to 2 Gy-WBI or 2 Gy-PBI. The list of commonly deregulated miRNA is also reported. Data were obtained by triplicate samples.

Proteome analysis of the organ exosomes 24 hours after PBI or WBI

Whole brain exosomes: The principal component analysis (PCA) based on all proteomic features of the brain exosome proteomes after 2 Gy PBI and 2 Gy WBI showed that both irradiation types differed from the sham-irradiated control but also from each other (Fig. 9A). The proteomics analysis showed that 28 and 119 proteins were significantly deregulated in exosomes 24 hours after 2 Gy PBI and 2 Gy WBI, respectively (Fig. 9B) indicating that the number of altered proteins increased markedly if the irradiation included the whole body. Especially in the case of WBI, the upregulated proteins represented the majority of all deregulated proteins whereas this was not so clear in the case of PBI (94%/WBI; 64%/PBI). Most deregulated proteins were typical brain proteins and could be categorised to neuronal or synaptic functions. Among deregulated proteins, 19 proteins were common between the two radiation modalities (Fig. 9C). These 19 proteins formed two interactive clusters (Fig. 9D) and represented KEGG pathways “Synaptic vesicle cycle”, “Metabolic pathways”, “Glycolysis/Gluconeogenesis” (Fig. 9E). In addition, other metabolic pathways (“Ether lipid metabolism”, “Propanoate metabolism”) were among the most significant pathways. The association of the common proteins with the KEGG pathways was statistically significant ($p<0.05$).

Next, the deregulated proteins from PBI and WBI were analysed separately. The STRING protein-protein interaction analysis showed little clustering in the case of PBI (Figure 9F). Most of the deregulated proteins belonged to cytoplasmic or plasma membrane proteins but also presynaptic and axon terminal proteins were represented (Fig. 9G). The deregulated proteins after WBI were well clustered indicating a high degree of interaction (Fig. 9H). Most proteins belonged to myelin sheet or were synaptic or neuronal proteins (Fig. 9I).

The prediction analysis of the upstream regulators of the deregulated proteins was performed using the Ingenuity Pathway Analysis. Due to the small number of deregulated proteins after PBI (n=28), no prediction of activation or inactivation of transcriptional regulators was possible. However, the transcription factor CREB was shown as a possible regulator with no activation status (data not shown). In the case of WBI, several predicted regulators were found, namely APP (Fig. 9J); BDNF (Fig. 9L), and CREB1 (Fig. 9M) were predicted to be activated whereas FMR1 (Fig. 9K) was predicted to be inactivated in the irradiated brain.

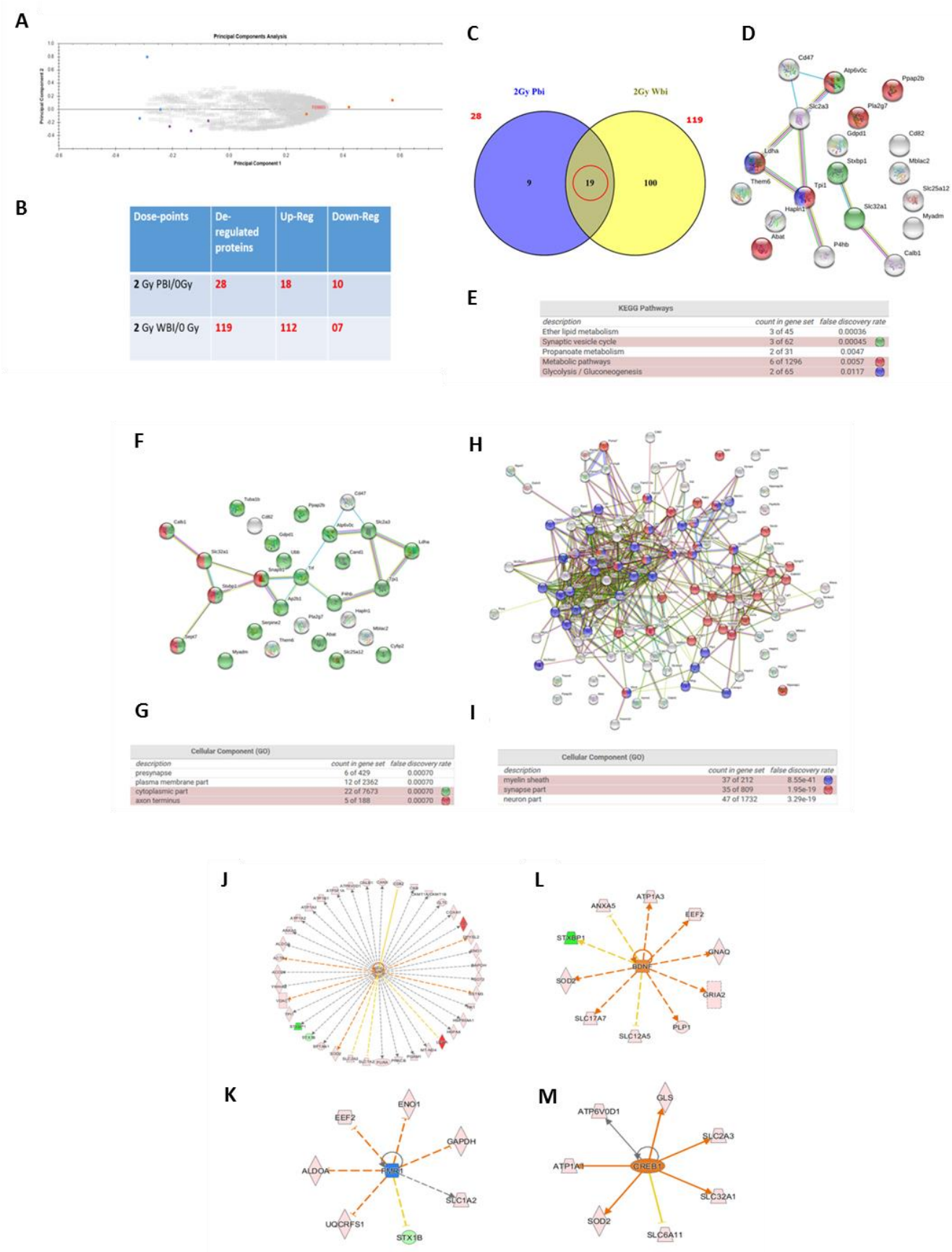

Dose-points	De-regulated proteins	Up-Reg	Down-Reg
2 Gy PBI/0Gy	28	18	10
2 Gy WBI/0 Gy	119	112	07

Fig. 9. Characterisation of the exosomal proteomes from the brain 24 hours after WBI and PBI. The PCA (**A**) shows the separation of the different doses at 0 Gy (blue), 2 Gy PBI (purple), and 2 Gy WBI (orange). The table (**B**) shows the number of significantly deregulated, up-regulated and down-regulated proteins in exosomes isolated from the brain of mice exposed to PBI or WBI in comparison to controls. The Venn diagram (**C**) shows the number of significantly deregulated and common

proteins in exosomes from 2 Gy PBI and 2 Gy WBI compared to controls and a STRING interaction analysis (**D**) shows the clustering of common proteins. The table of the most significant KEGG pathways represented by the common proteins is shown (**E**). The protein-protein interaction analysis using STRINGdb of all deregulated brain exosomal proteins after 2 Gy PBI is shown (**F**). The GO "Cellular component" analysis indicating the cellular localisation of all deregulated proteins (PBI) is shown (**G**). The protein-protein interaction analysis using STRINGdb of all deregulated brain exosomal proteins after 2 Gy WBI showed marked clustering (**H**). The GO "Cellular component" analysis of all deregulated proteins after WBI indicated myelin, synaptic or neuronal involvement (**I**). Based on all deregulated proteins, an activation (orange colour) of amyloid precursor protein (APP) (**J**), brain-derived neurotrophic factor (BDNF) (**L**), and cAMP response element-binding protein (CREB) (**M**) was predicted using Ingenuity Pathway Analysis. Fragile X mental retardation protein (FMR1) was predicted to be inactivated (blue colour) (**K**).

Liver exosomes: The principal component analysis (PCA) based on all proteomic features of the liver exosome proteomes after 2 Gy PBI and 2 Gy WBI showed that both irradiation types differed from the sham-irradiated control but also from each other (Fig. 10A). The proteomics analysis showed that 303 and 153 proteins were significantly deregulated in exosomes 24 hours after 2 Gy PBI and 2 Gy WBI, respectively (Fig. 10B) indicating that the number of altered proteins increased markedly after partial body exposure. Majority of all deregulated proteins in liver exosome proteome after PBI were down-regulated whereas this was not so clear in the case of WBI.
Among deregulated proteins, 92 proteins were common between the two radiation modalities (Fig. 10C). These 92 proteins formed three main clusters (Fig. 10D) mainly involved in the mitochondrial oxidation-phosphorylation (in red), ER cytochrome 450 metabolism (in green) and proteasome activity (in blue). Next, the deregulated proteins from PBI and WBI were analysed separately. The mitochondrial oxidation-phosphorylation, ER cytochrome 450 and proteasome signalling pathways were mainly affected in by radiation in the exosome proteomes (Fig. 10E and 10F).

Heart exosomes: The principal component analysis (PCA) based on all proteomic features of the heart exosome proteomes after 2 Gy PBI and 2 Gy WBI emphasized that the proteome response of the irradiated samples (PBI and WBI) differed neither from each other nor from the sham-irradiated controls (Fig. 11A). The proteomics analysis showed only 9 proteins that were significantly deregulated in exosomes 24 hours after 2 Gy PBI. No proteins qualified by statistical criteria in proteome profile of heart exosomes after 2 Gy WBI (Fig. 11B), mainly due to the considerable variance of the sham-irradiated samples.

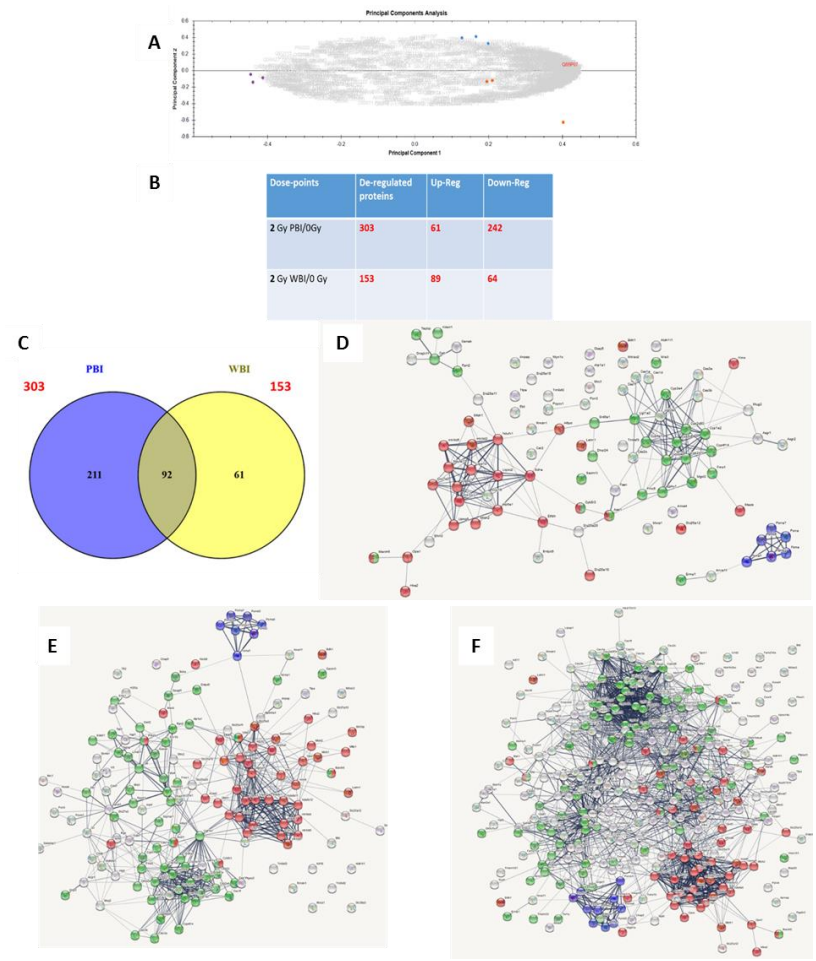

Fig. 10. Characterisation of the exosomal proteomes from the liver 24 hours after WBI and PBI. The PCA (**A**) shows the separation of the different doses at 0 Gy (blue), 2 Gy PBI (purple), and 2 Gy WBI (orange). The table (**B**) shows the number of significantly deregulated, up-regulated and down-regulated proteins in exosomes isolated from the liver of mice exposed to PBI or WBI in comparison to controls. The Venn diagram (**C**) shows the number of significantly deregulated and common proteins in exosomes from 2 Gy PBI and 2 Gy WBI compared to controls. A STRING interaction analysis (**D**) shows the clustering of common proteins. The protein-protein interaction analysis using STRINGdb of all deregulated brain exosomal proteins after 2 Gy WBI (**E**) and PBI (F) is shown.

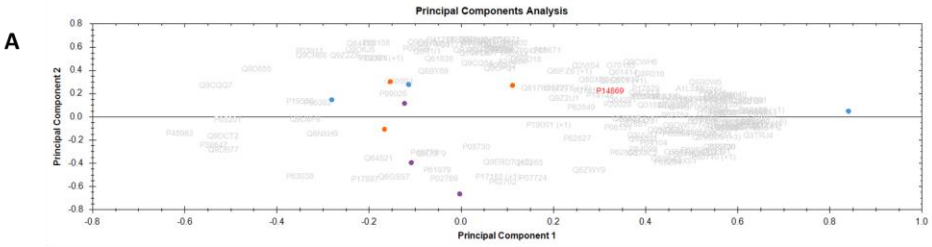

B

Dose-points	De-regulated proteins	Up-Reg	Down-Reg
2 Gy PBI/0Gy	9	1	8
2 Gy WBI/0 Gy	0	0	0

Fig. 11. **Characterisation of the exosomal proteomes from the whole heart 24 hours after the exposure**. The PCA (**A**) shows the separation of the different doses at 0 Gy (blue), 2 Gy PBI (purple), and 2 Gy WBI (orange). The table (**B**) shows the number of significantly deregulated, up-regulated and down-regulated proteins in exosomes isolated from the heart of mice exposed to PBI or WBI in comparison to controls.

Proteome analysis of the organ exosomes 15 days after PBI or WBI

Brain exosomes: In the exosomes from whole brain 15 days after exposure to ionizing radiation 707 proteins were identified, of which 333 were identified with at least 2 unique peptides. The PCA analyses based on all proteomic features suggested a difference between the sham-irradiated group and PBI and WBI groups (Fig. 12A). There was a close clustering observed in the PBI group compared to sham-irradiated or whole-body irradiated groups. Nevertheless, also the WBI group was clearly separated from the controls.

There were 48 significantly deregulated proteins in the PBI group and 86 in the WBI group (Fig. 12B). The majority of the deregulated proteins in the WBI group were upregulated (74) whilst in the PBI group the number of up- and downregulated proteins was similar (21/27).

There were 37 commonly deregulated proteins identified in the brain exosomes isolated after WBI or PBI (Fig. 12C). Most of these common proteins were involved in the biological processes 'regulation of biological quality (GO:0065008)', 'localization (GO:0051179)', and 'neuron differentiation (GO:0030182)' (Fig. 12D and 12E).

A

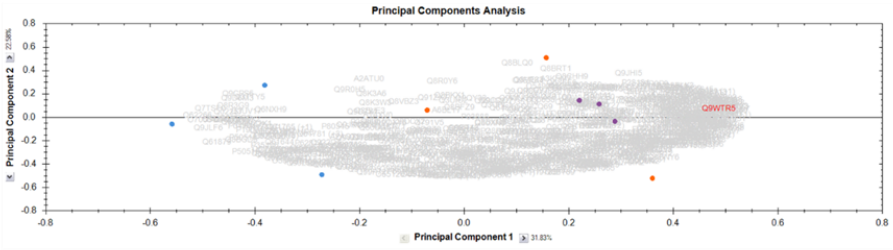

B

Dose-points	De-regulated proteins	Up-Regulated	Down-Regulated
2 Gy PBI/0Gy	48	21	27
2 Gy WBI/0 Gy	86	74	12

C

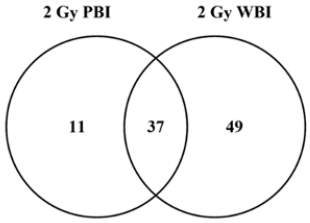

D

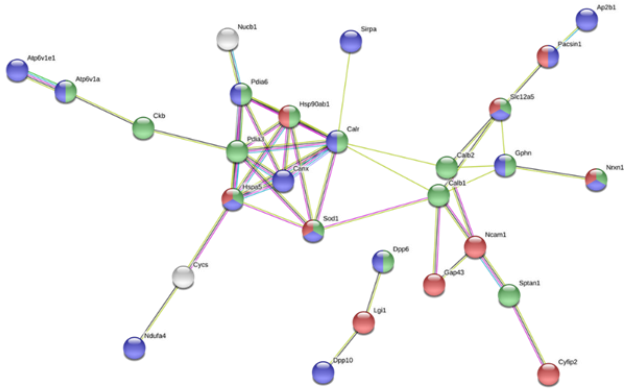

E

Biological Process (GO)

GO-term	description	count in gene set	false discovery rate
GO:0065007	biological regulation	32 of 10168	0.00061
GO:0031175	neuron projection development	9 of 637	0.00067
GO:0072657	protein localization to membrane	7 of 336	0.00071
GO:0065008	regulation of biological quality	18 of 3420	0.00092
GO:0120036	plasma membrane bounded cell projection organization	10 of 982	0.0010
GO:0060341	regulation of cellular localization	9 of 811	0.0010
GO:0051641	cellular localization	13 of 1792	0.0010
GO:0051179	localization	20 of 4315	0.0010
GO:0051049	regulation of transport	13 of 1782	0.0010
GO:0030182	neuron differentiation	10 of 973	0.0010

Fig. 12. **Characterisation of the exosomal proteomes from the brain 2 weeks after WBI and PBI**. The PCA (**A**) shows the separation of the different doses at 0 Gy (blue), 2 Gy PBI (purple), and 2 Gy WBI (orange). The table (**B**) shows the number of significantly deregulated, up-regulated and down-regulated proteins in exosomes isolated from brain of mice exposed to PBI or WBI in comparison to controls. The common deregulated proteins identified between PBI and WBI groups are presented in the Venn diagram (**C**). Protein-protein interaction analysis performed by STRINGdb is shown (**D**). Proteins belonging to 'regulation of biological quality' are shown in green, proteins belonging to 'localization' in blue and proteins belonging to 'neuron differentiation' in red. The table of the most significant biological processes from the Gene Ontology (GO) knowledgebase for the commonly deregulated proteins is shown (**E**).

Liver exosomes: The PCA based on all proteomic features revealed a difference in the exosomes isolated from the liver in the sham-irradiated mice compared to those of mice that were exposed to 2 Gy PBI or WBI (Fig. 13A). A strong clustering was observed for the sham-irradiated control group.
In the liver exosomes, 1477 proteins were identified, 918 of which were identified with more than one unique peptides (Fig. 13B). There were 202 and 564 proteins significantly deregulated in the liver exosomes of mice that were exposed to PBI and WBI, respectively. This indicated a dose-dependent increase in the deregulated exosomal proteins. In the case of PBI, the majority (153) of deregulated proteins were down-regulated whilst in the WBI group the number of up-regulated and down-regulated proteins was similar (294/270).
In the significantly deregulated protein group, 139 proteins were commonly deregulated in liver exosomes after PBI and WBI (Figure 13C). Protein-protein network analysis performed with STRINGdb revealed several clusters that were interconnected. Similar to the liver exosomes at 24-hour time point, a very well interconnected cluster included proteins of the proteasome complex. At both time points, the proteins of the proteasome were down-regulated in the case of PBI but up-regulated in the case of WBI. Most of the proteins were involved in the biological processes of 'oxidation-reduction process (GO:0055114)', 'small molecule metabolic process (GO:0044281)', and 'drug metabolic process (GO:0042775)' (Figure 13D, 13E).

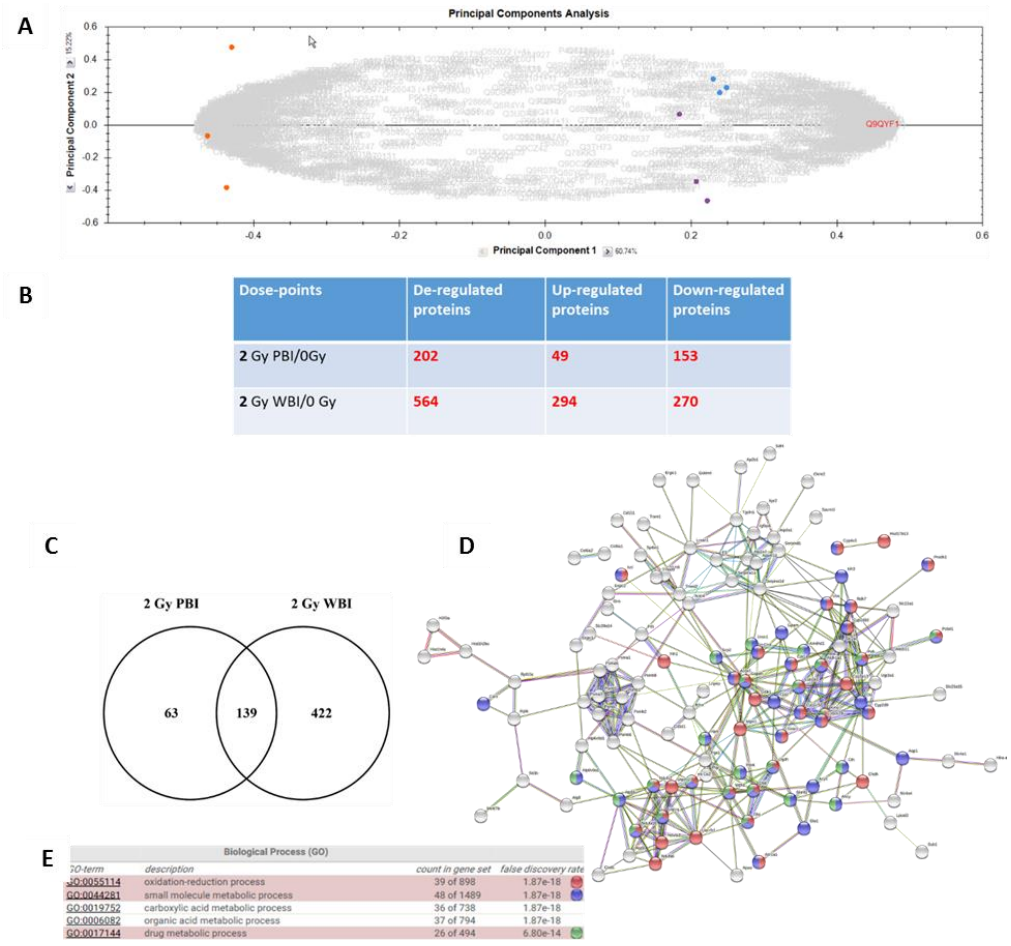

Dose-points	De-regulated proteins	Up-regulated proteins	Down-regulated proteins
2 Gy PBI/0Gy	202	49	153
2 Gy WBI/0 Gy	564	294	270

Fig. 13. **Characterisation of the exosomal proteomes from the liver 2 weeks after WBI and PBI**. The PCA (**A**) shows the separation of the different doses at 0 Gy (blue), 2 Gy PBI (purple), and 2 Gy WBI (orange). The table (**B**) shows the number of significantly deregulated, up-regulated and down-regulated proteins in exosomes isolated from hearts of mice exposed to PBI or WBI in comparison to controls. The common deregulated proteins identified between PBI and WBI groups are presented in the Venn diagram (**C**). A protein-protein interaction analysis performed by STRINGdb is shown (**D**). Proteins belonging to 'drug metabolic process' are shown in green, proteins belonging to 'small molecule metabolic process' are shown in blue, and proteins belonging to 'oxidation-reduction process' are shown in red. The most significant biological processes (GO) for the commonly deregulated proteins are shown (**E**).

Heart exosomes: The PCA based on all proteomic features suggested that the heart exosomes isolated from the sham-irradiated control group differed from those isolated from PBI or WBI exposed mice (Fig. 14A). There was less variation within the WBI group compared to the other two groups. In the heart exosomes, 183 proteins were identified, of which 99 were identified with at least two unique peptides (Fig. 14B). There were 15 proteins that were commonly significantly deregulated in the heart exosomes at 2 Gy PBI or WBI (Fig. 14C). A protein-protein network analysis (STRINGdb) indicated a cluster originating from the inner mitochondrial membrane consisting of proteins from the respiratory chain. These proteins are down-regulated after PBI and WBI. Most of the common proteins were involved in the biological processes of 'ATP synthesis coupled electron transport (GO:0042773)', 'cellular respiration (GO:0045333)', and 'mitochondrial ATP synthesis coupled electron transport (GO:0042775)' (Fig. 14D, 14E).

A

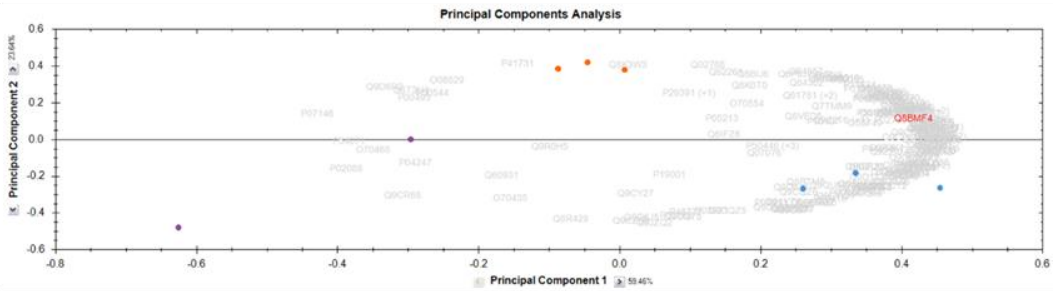

B

Dose-points	De-regulated proteins	Up-regulated proteins	Down-regulated proteins
2 Gy PBI/0Gy	29		29
2 Gy WBI/0 Gy	52	2	50

C

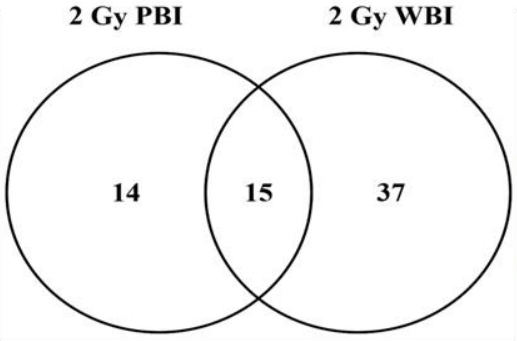

D

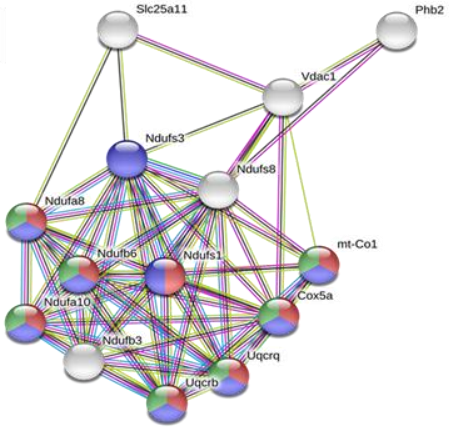

E

Biological Process (GO)			
GO-term	*description*	*count in gene set*	*false discovery rate*
GO:0042773	ATP synthesis coupled electron transport	8 of 56	8.79e-15
GO:0022900	electron transport chain	9 of 120	8.79e-15
GO:0045333	cellular respiration	9 of 140	1.21e-14
GO:0006091	generation of precursor metabolites and energy	10 of 295	4.52e-14
GO:0042775	mitochondrial ATP synthesis coupled electron transport	7 of 51	2.06e-13

Fig. 14. **Characterisation of the exosomal proteomes from the heart 2 weeks after WBI and PBI**. The PCA (**A**) shows the separation of the different doses at 0 Gy (blue), 2 Gy PBI (purple), and 2 Gy WBI (orange). The table (**B**) shows the number of significantly deregulated, up-regulated and down-regulated proteins in heart exosomes in mice exposed to PBI or WBI in comparison to controls. The common deregulated proteins identified between PBI and WBI groups are presented in the Venn diagram (**C**). Protein-protein interaction analysis performed by STRING is shown (**D**). Proteins belonging to 'mitochondrial ATP synthesis coupled electron transport' are shown in green, proteins belonging to 'cellular respiration' areshown in blue, and proteins belonging to 'ATP synthesis coupled electron transport' is shown in red. The table of the most significant biological processes according to GO for the commonly deregulated proteins is shown (**E**).

In summary, these findings show that the exosome cargo from different organs (whole brain, liver, heart) is primarily organ-specific. In the brain, the exosomal proteins mainly belong to brain-specific compartments such as myelin sheaths, synapses or axons, while in the liver many exosomal proteins belong to the category cytochrome P450 proteins (CYPs) and in the heart to the mitochondrial proteins.
In the brain exosomes, differences were found in the response at 24-hour and 15 days post-irradiation, indicating a rapid adjustment of this organ. The number of deregulated exosomal proteins increases considerably when comparing PBI to WBI at both time points. The liver exosomes show at both time points and radiation modalities similar changes in their cargo including the aforementioned CYPs but also many proteins of the proteasome complex. Interestingly, the proteins of the proteasome complex are down-regulated at PBI but up-regulated at WBI at both time points. For the heart exosomes, a comparison of the two time points was not relevant since the statistical analysis was not possible at 24-hour. A down-regulation of respiratory chain proteins was the most prominent feature at 15 days.

Raman spectral analysis of the organ and plasma exosomes after PBI or WBI

Principal Component Analysis – Linear Discriminant Analysis (PCA-LDA) showed that spectra from exosomes from brain and liver from control, WBI and PBI mice 24 hours after irradiation could be clearly discriminated (Fig. 15). Good quality Raman spectra could not be obtained from the exosomes from heart at 24 hours after irradiation.

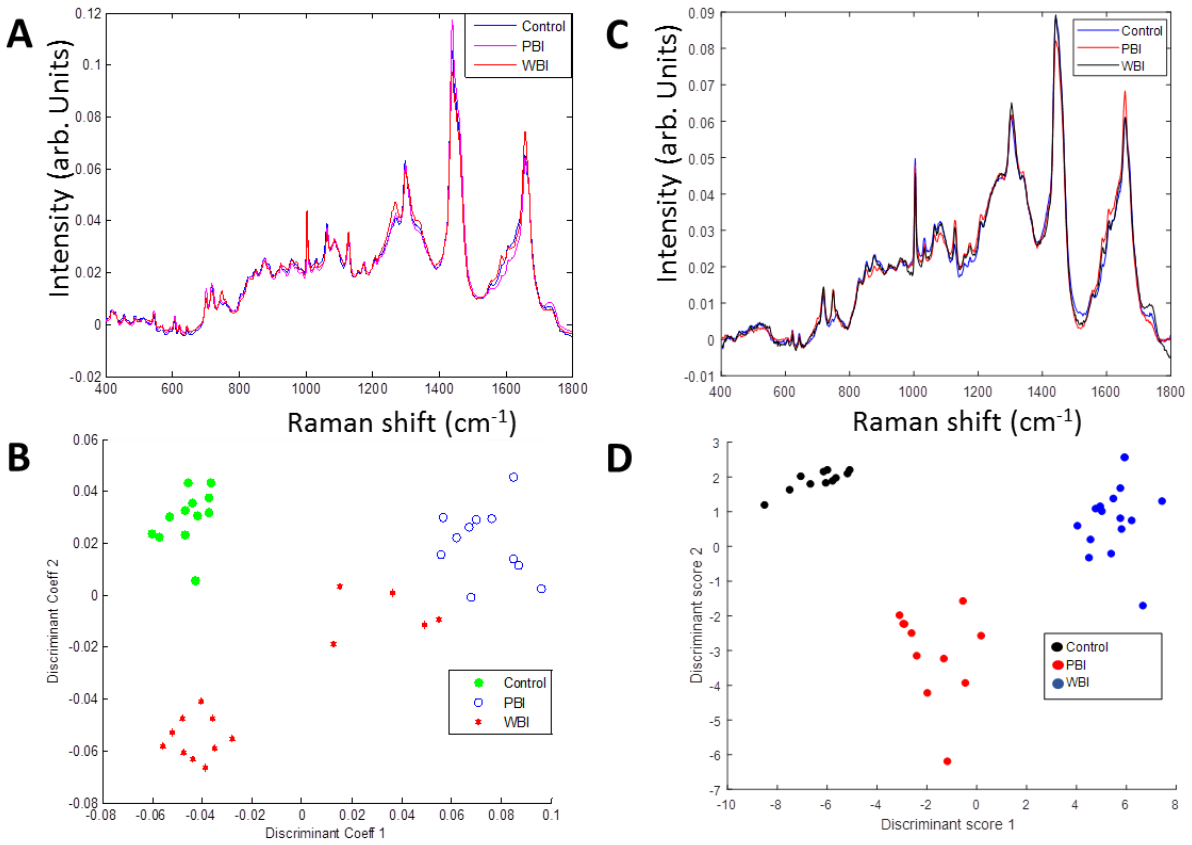

Fig. 15. (**A**) Mean Raman spectra from exosomes from brain of control, PBI and WBI mice at 24 hours post irradiation, (**B**) PCA-LDA scatterplot of Raman spectral data from exosomes from control (green), PBI (blue) and WBI (red) brain showing good separation of the groups, (**C**) Mean Raman spectra from exosomes from liver of control, PBI and WBI mice at 24 hours post irradiation, (**D**) PCA-LDA scatterplot of Raman spectral data from exosomes from control (black), PBI (red) and WBI (blue) liver showing good separation of the groups.

PCA-LDA showed that spectra from exosomes from brain from control, WBI and PBI mice 15 days after irradiation could be clearly discriminated while spectra from exosomes from heart and liver clustered into control and irradiated (PBI and WBI) groups (Fig. 16).

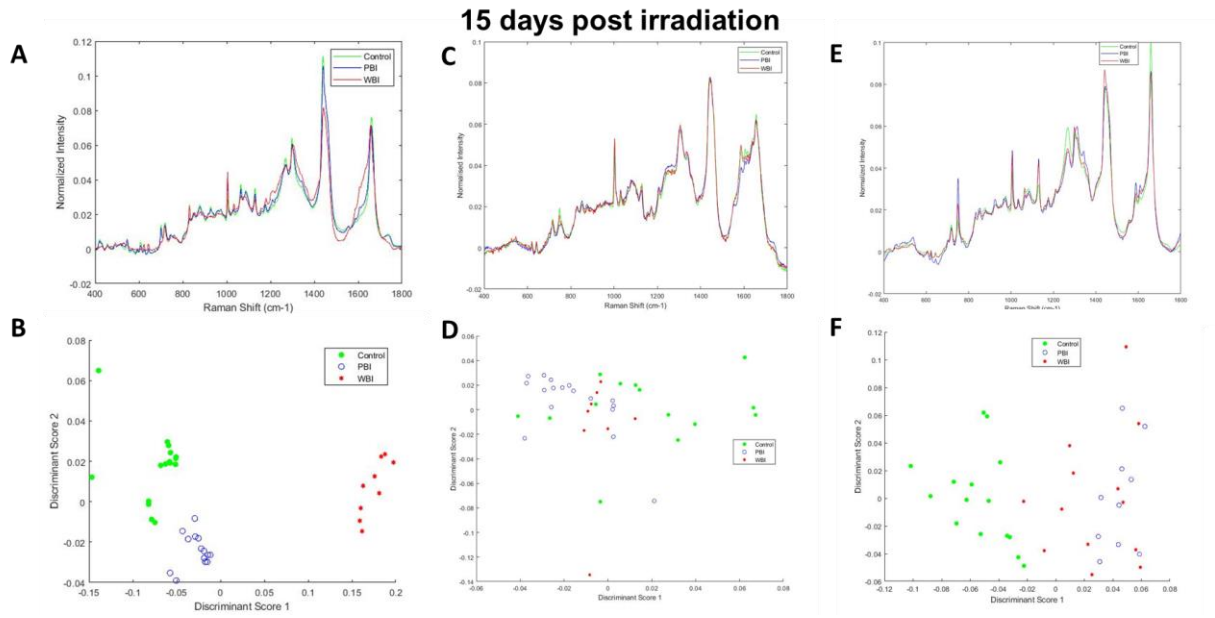

Fig. 16. (**A**) Mean Raman spectra from exosomes from brain of control, PBI and WBI mice at 15 days post irradiation, (**B**) PCA-LDA scatterplot of Raman spectral data from exosomes from control (green), PBI (blue) and WBI (red) brain showing good separation of the groups, (**C**) Mean Raman spectra from exosomes from heart of control, PBI and WBI mice at 15 days post irradiation, (**D**) PCA-LDA scatterplot of Raman spectral data from exosomes from control (green), PBI (blue) and WBI (red) liver showing good separation of the control and PBI/WBI groups. (**E**) Mean Raman spectra from exosomes from liver of control, PBI and WBI mice at 15 days post irradiation, **(B**) PCA-LDA scatterplot of Raman spectral data from exosomes from control (green), PBI (blue) and WBI (red) brain showing good separation of the control and PBI/WBI groups.

Good quality Raman spectra could not be obtained from the exosomes from plasma at 24 hours after irradiation due to contamination with haemoglobin which has a strong Raman signature and masked the spectral features from the exosomes (Fig. 17).

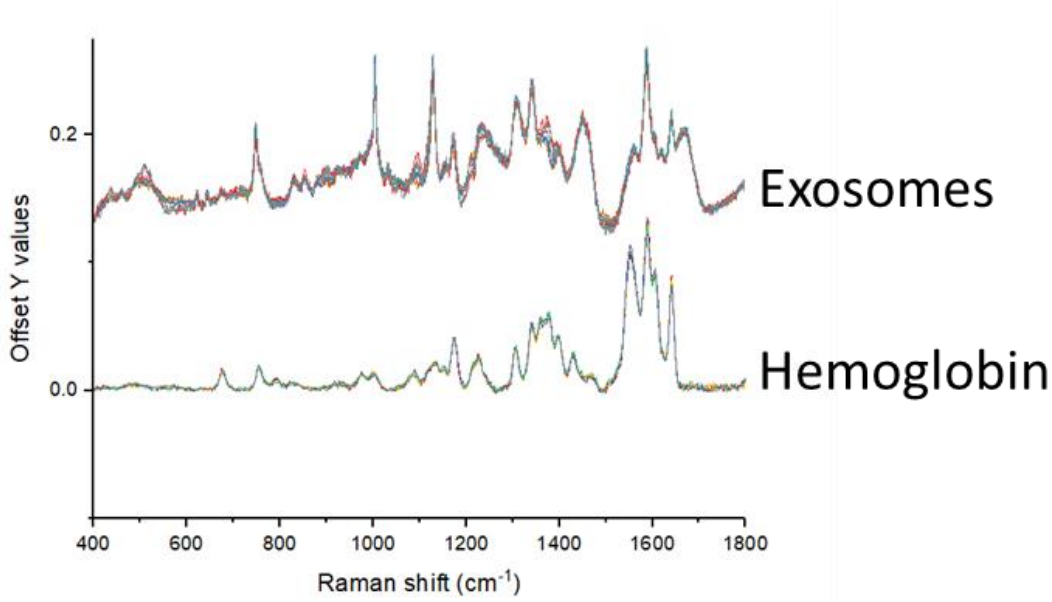

Fig. 17. Representative Raman spectra from exosomes from plasma of control mice (top), Raman spectra from hemoglobin (bottom)

Task 3.2 *In vitro* functional effects (OBU, TU)

Here we investigated the exosome-mediated radiation signaling by transferring exosomes from both 2Gy WBI or PBI mice to recipient mouse embryonic fibroblast (MEF) cells and evaluating their effect on cellular viability and DNA damage compared to that of exosome derived from control mice.

Effects of exosomes on MEF viability

We here assessed whether transfer of exosomes derived from 2Gy WBI or PBI organs and plasma was able to influence cell viability in MEFs.

Results showed that transfer of exosomes collected 24 hours postirradiation from 2Gy WBI brain, 2Gy WBI liver, 2Gy PBI liver and 2Gy PBI heart significantly reduced viability of MEF cells, while transfer of plasma-derived exosomes did not significantly affect cell viability (Fig. 18A).

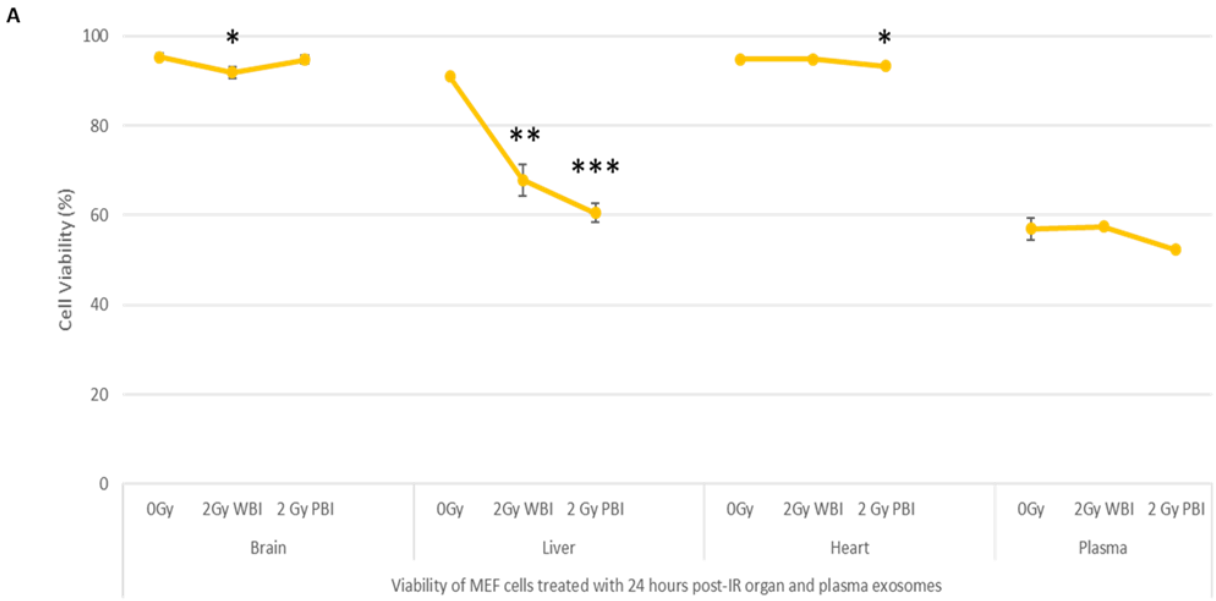

Fig. 18. **Effect of exosome-transfer on MEFs cell viability**. Viability of MEF cells treated with 24h post- exosomes obtained from organs and plasma of 2Gy WBI or PBI mouse compared to unirradiated mouse organ and plasma exosomes. Data groups were obtained by triplicate measurements.

DNA damage effects of Exosomes on MEF cells Comet Assay

In order to asses if transfer of exosomes obtained from 2Gy WBI or PBI organs was able to induce DNA damaging effects on MEF cells we measured the DNA damage in the comet tail (Fig.19).
A significant increase in DNA damage was observed after transfer of exosomes derived from 2 Gy PBI brain, liver and plasma at 24 hours post-irradiation compared to other experimental groups. For brain, liver and heart samples, highest DNA damage was observed in MEF cells treated with 24 hours 2Gy WBI mice exosomes while treatment with plasma exosomes from both 2Gy WBI and PBI mice caused significantly higher DNA damage in MEF cells compared to unirradiated control treated MEF cells.

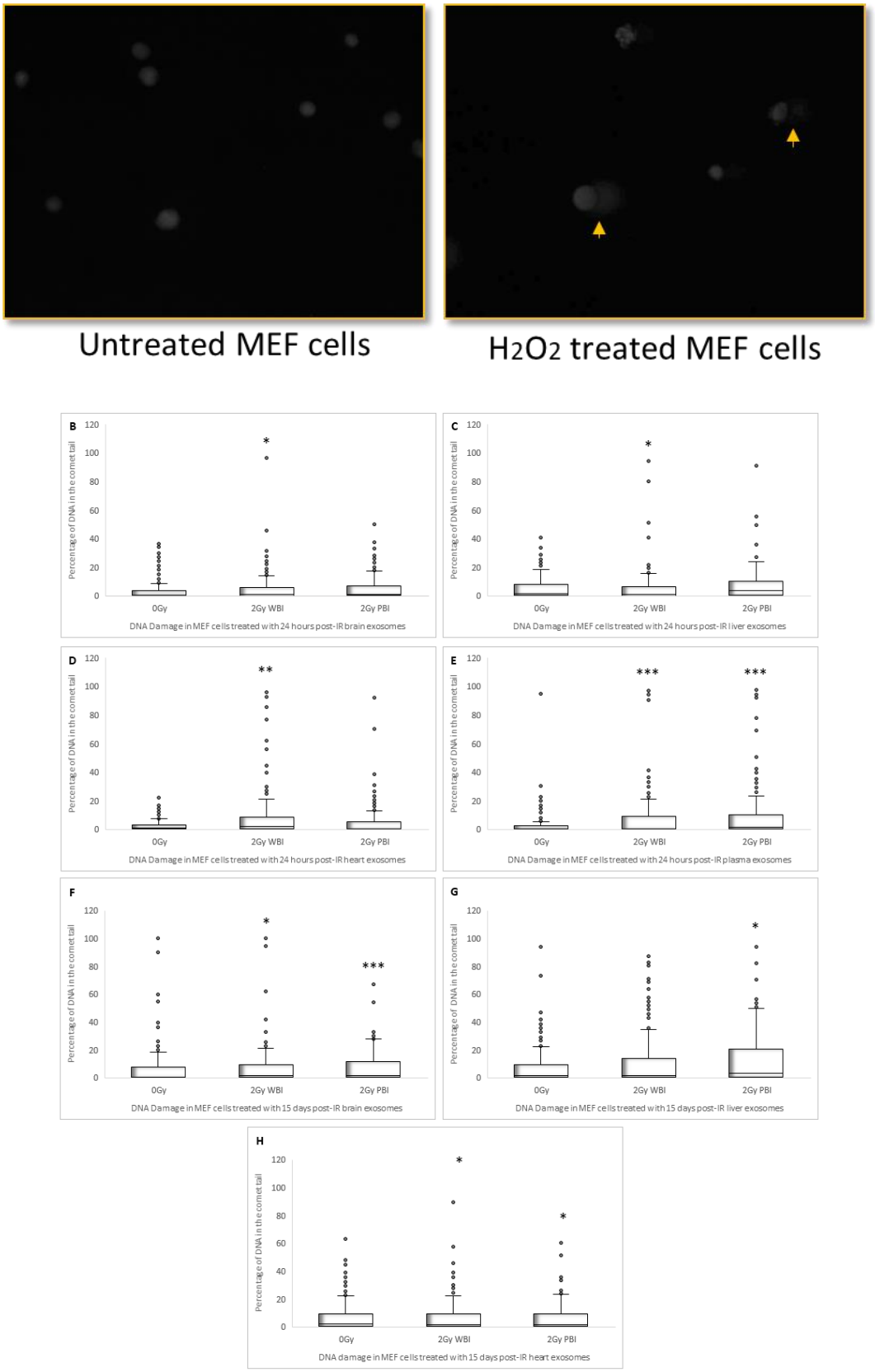

Fig. 19. Induction of DNA damage in MEF cells. (**A**) Comet tail representation for untreated or H2O2 treated MEF cells. MEFs treated with 24 hours post-IR exosomes (**B-E**) and 15 days post-IR (**F-H**) obtained from organs, and plasma of 2Gy WBI or PBI mice compared DNA damage in MEF cells treated with from unirradiated mice organ exosomes. Percentages of DNA in the comet tail were scored in 200 cells treated for each group. Statistical analysis was performed using Mann-Whitney U Test (*$p < 0.05$, **$p < 0.01$, ***$p < 0.001$).

Similarly, a significant increase in DNA damage was also observed in MEF cells treated with 15 days post-IR 2Gy WBI and PBI brain; 2Gy PBI liver and 2Gy WBI and PBI heart exosomes compared to their corresponding controls treated with unirradiated exosomes.

γH2AX immunostaining

To further evaluate DNA damage in terms of double strand breaks (DSBs), γH2AX immunostaining was carried out in MEF treated with exosomes derived from organ and plasma of 2Gy-PBI, 2Gy-WBI or unirradiated mice both at 24 hour and 15 day after exposure (Fig. 20 and Fig.21).

Although DSBs were significantly increased in MEFs treated with organs-derived (brain, liver, heart) and plasma-derived exosomes at 24 hours post-irradiation, the highest DSBs level was observed in MEF cells treated with brain-derived exosomes. Instead, γH2AX foci were not significantly increased after transfer of exosomes isolated at 15 days post-irradiation, showing that the exosome ability to induce DSBs is transient.

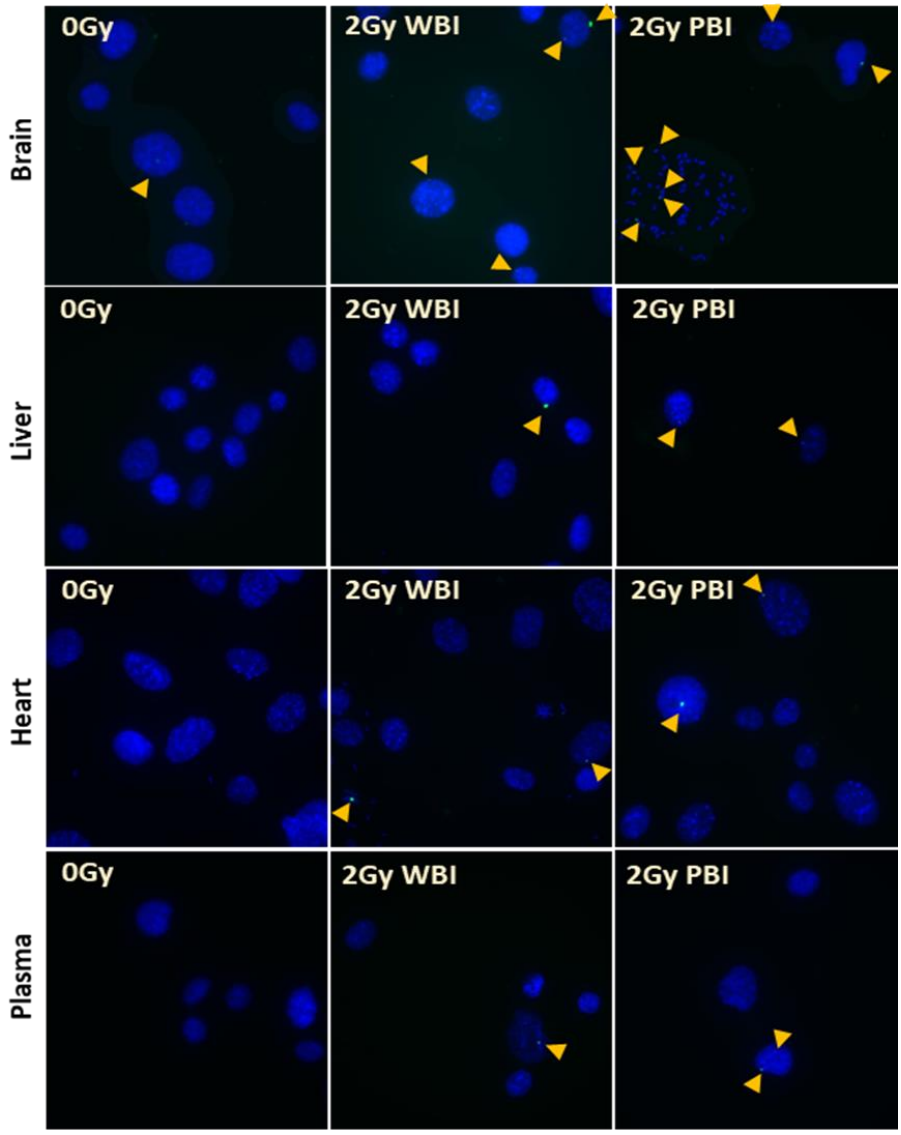

Fig. 20. γH2AX foci formation in MEFs treated with exsosomes derived from organs and plasma at 24 hours post-irradiation. Representative 63X fluorescent microscope images of MEF cells treated with 24 hours post-IR exosomes obtained from organs and plasma. Arrows indicate the location of γH2AX foci (Alexa488). Cells were counterstained with DAPI.

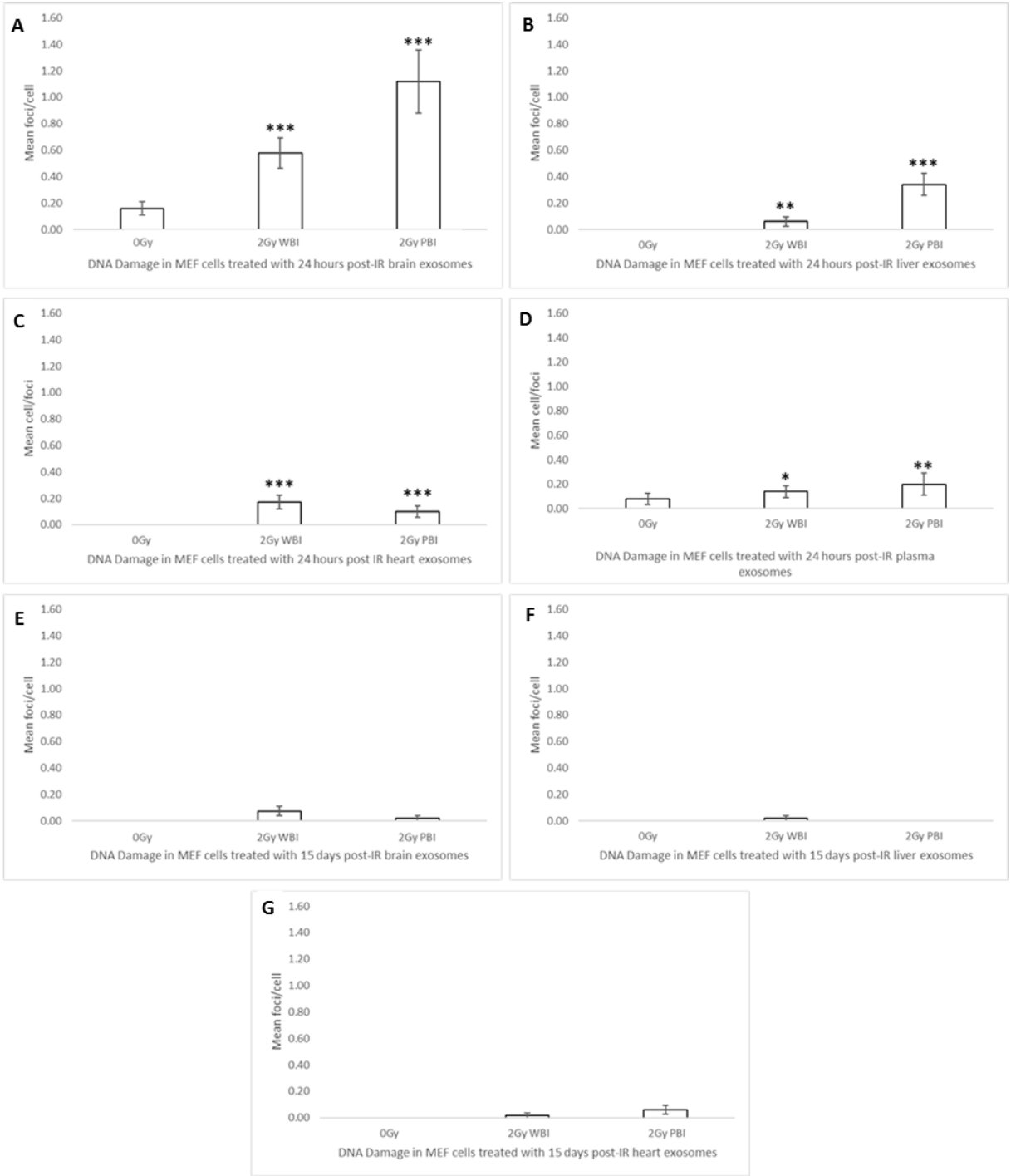

Fig. 21. Effect of transfer of exosomes isolated from organ and plasma of 2Gy-WBI or 2Gy-PBI mice compared to organ exosomes from unirradiated mice in MEFs. Bars represent the mean γH2AX foci formed per cell ± SEM treated with 24 hours post-IR organ and plasma exosomes (**A-D**) and 15 days post-IR organ exosomes (**E-G**). Significance was tested by Fisher's exact test. (*p < 0.05, **p < 0.01, ***p < 0.001).

Analysis of chromosome aberrations

Chromosomal damage was assessed in metaphase chromosomes of MEF cells treated with 24 hours post-IR exosomes and 15 days post-IR exosomes (Fig. 22). Chromosomal aberrations were significantly increased in MEF treated with WBI brain, heart and plasma and PBI liver exosomes compared to MEF cells treated with control organs and plasma exosomes. Chromosomal aberrations were not significantly different between treatment groups for MEF cells treated with 15 days post-IR exosomes.

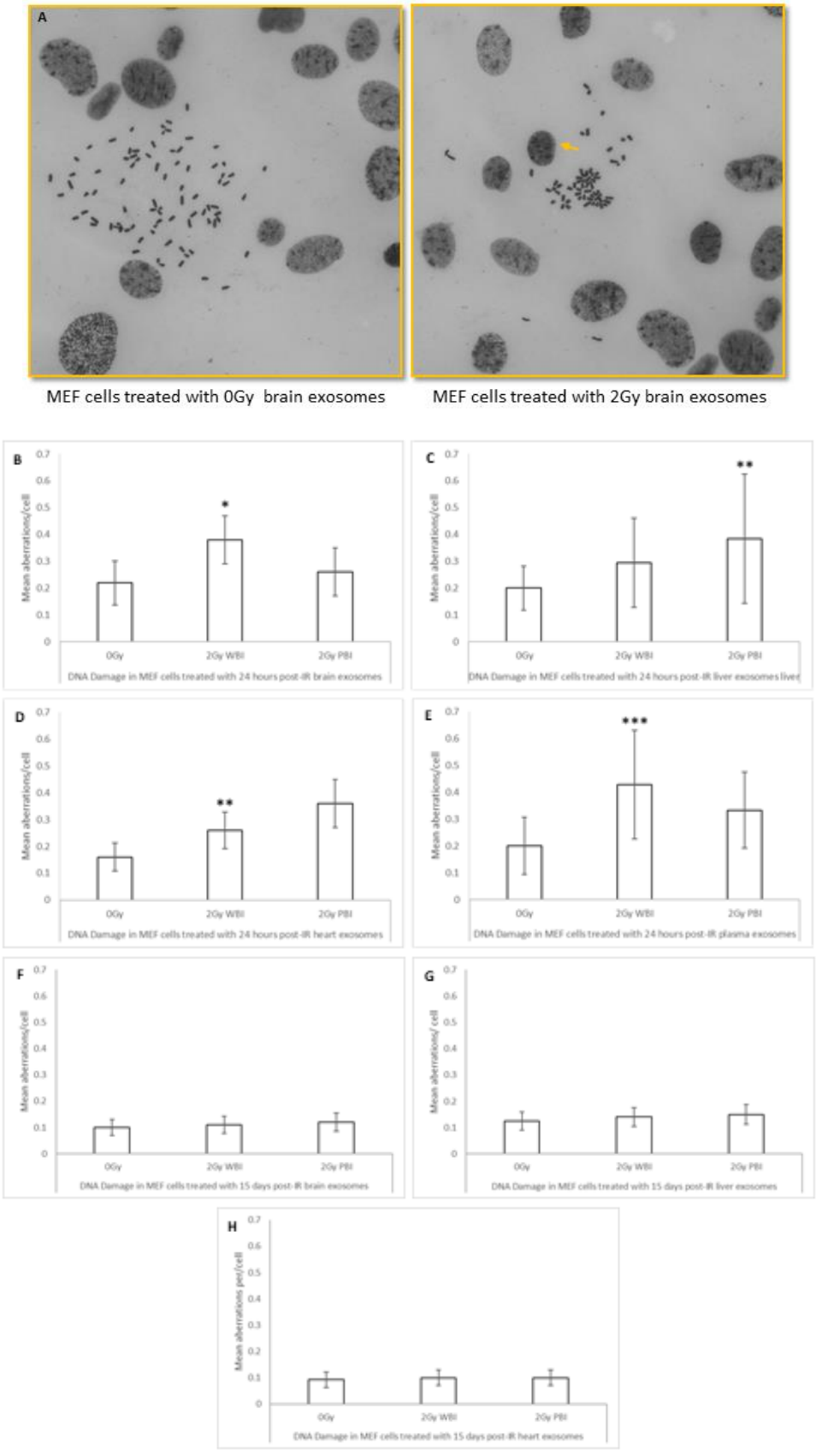

Fig. 22. Chromosomal aberrations in MEFs. (**A**) Cells treated with 24h post IR (**B-E**) and 15 days post-IR (**F-H**) exosomes obtained from organs and plasma of 2Gy WBI or PBI mouse compared to corresponding unirradiated mouse organ exosomes. Chromosomal aberrations (total) were scored in 100 metaphase spreads in cells treated with corresponding exosomes for 24h. Bars represent mean chromosomal aberrations per cell ± SEM; significance was tested by Fisher's exact test. (*$p < 0.05$, **$p < 0.01$, ***$p < 0.001$).

Effects of exosomes transfer on calcium signalling

Evaluation of intracellular calcium show that rapid calcium fluxes were induced in MEF recipient cells following addition of exosomes from brain, heart and liver from WBI and PBI mice but not from sham irradiated mice at 24 hours and 15 days post irradiation (Fig.23 A-F). Similarly, rapid calcium fluxes were induced in MEF recipient cells following addition of exosomes from plasma from WBI and PBI mice but not from sham irradiated mice at 24 hours post irradiation (Fig.23 G).

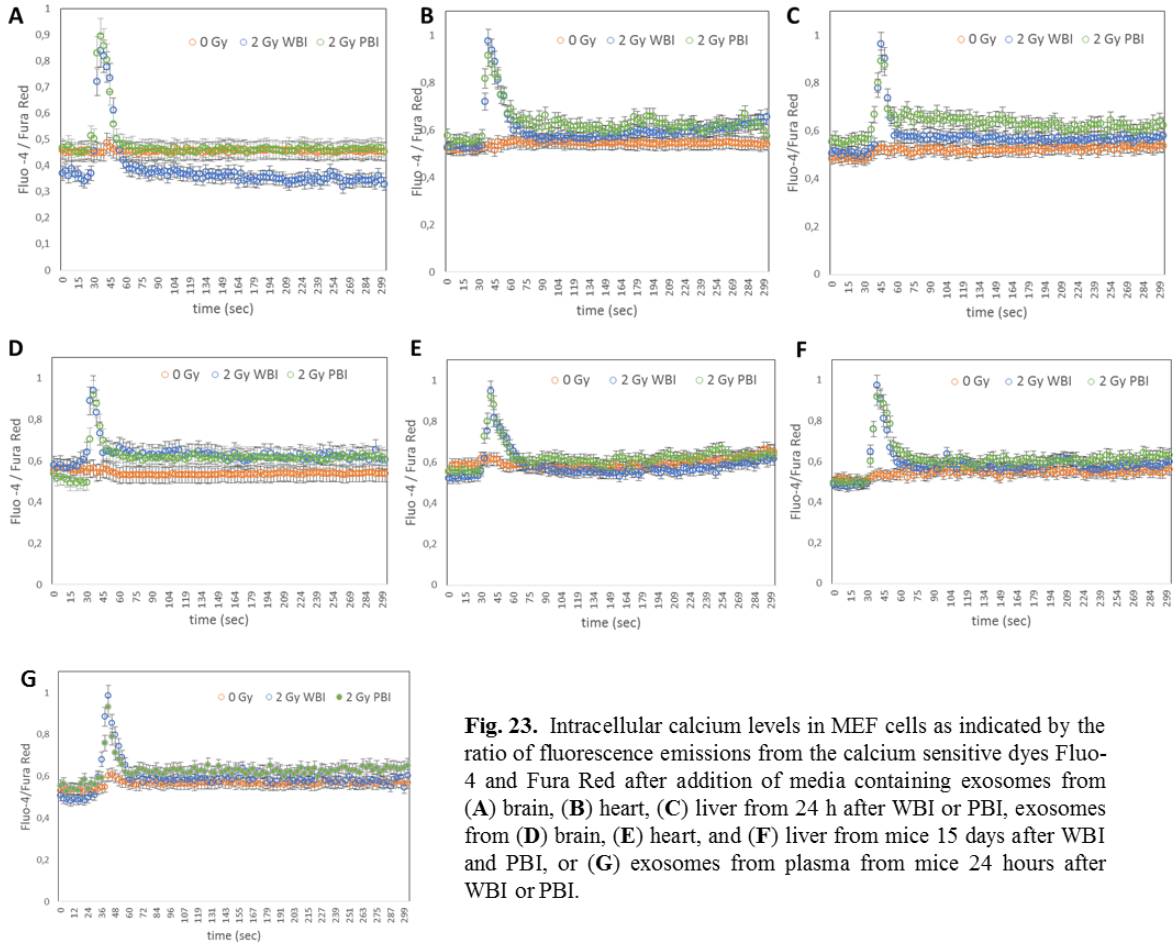

Fig. 23. Intracellular calcium levels in MEF cells as indicated by the ratio of fluorescence emissions from the calcium sensitive dyes Fluo-4 and Fura Red after addition of media containing exosomes from (**A**) brain, (**B**) heart, (**C**) liver from 24 h after WBI or PBI, exosomes from (**D**) brain, (**E**) heart, and (**F**) liver from mice 15 days after WBI and PBI, or (**G**) exosomes from plasma from mice 24 hours after WBI or PBI.

Effects of exosomes transfer on ROS/NO production

Production of ROS in MEF cells was measured using a fluorescent dye, CM-H2DCFDA. The data was expressed as mean fluorescence intensity normalised to each respective control. Significant ROS production was observed within 5 minutes of addition of exosomes from brain, heart and liver from WBI and PBI mice at 24 hours and 15 days post irradiation and within 5 minutes of addition of exosomes from plasma from WBI and PBI mice at 24 hours post irradiation (Fig. 24 A-C).

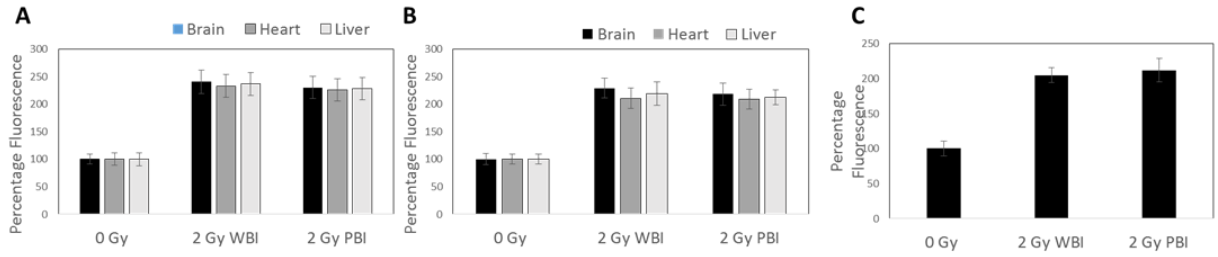

Fig. 24. Intracellular ROS levels in MEF cells as measured using CM-H2DCFDA fluorescence after addition of media containing exosomes from brain, heart and liver from mice (**A**) 24 hours and (**B**) 15 days after whole body (WBI) or partial body irradiation (PBI) and (**C**) from plasma from mice 24 hours after whole body (WBI) or partial body irradiation (PBI). Data is presented as mean ± SD after each sample was normalised to its respective control.

Similarly, NO levels were measured using a fluorescent dye, DAF. Again, the data was expressed as mean fluorescence intensity normalised to each respective control. Significant NO production was observed within 5 minutes of addition of exosomes from brain, heart and liver from WBI and PBI mice at 24 hours and 15 days post irradiation and within 5 minutes of addition of exosomes from plasma from WBI and PBI mice at 24 hours post irradiation (Fig. 25 A-C).

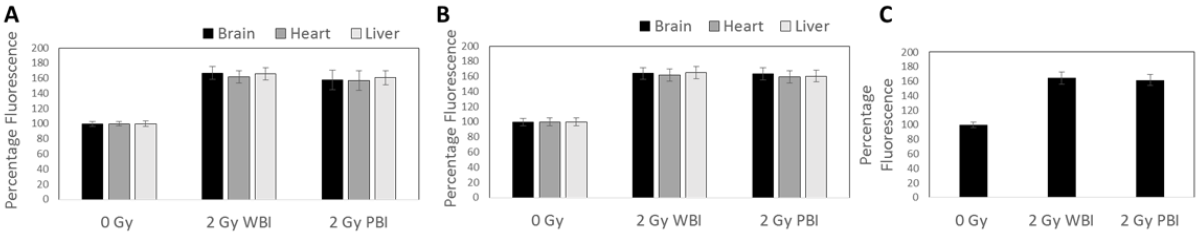

Fig. 25. Intracellular NO levels in MEF cells as measured using DAF fluorescence after addition of media containing exosomes from brain, heart and liver from mice (**A**) 24 hours and (**B**) 15 days after whole body (WBI) or partial body irradiation (PBI) and (**C**) from plasma from mice 24 hours after whole body (WBI) or partial body irradiation (PBI). Data is presented as mean ± SD after each sample was normalised to its respective control.

In summary, transfer of exosomes derived from organs at 24 hours post-irradiation from PBI and WBI mice to MEFs, significantly reduced cell viability, through the induction of DNA damage, as shown by γH2AX immunostaining, comet assay and chromosome analysis. Highest γH2AX foci levels were observed after treatment of MEFs with WBI and PBI brain exosomes at 24 h. Compared to organ-derived exosomes, plasma-derived exosomes were more effective in inducing DNA damage, as shown by the increased amount of DNA in comet tail and by the enhanced rate of total chromosome aberrations. Transfer of organ-derived exosomes from PBI and WBI mice at 15 days post-irradiation to MEFs, was also able to induce DNA damage as shown by the results of the comet assays. However, there was no significant increase of γH2AX foci or chromosomal aberrations in treated MEF cells indicating less overall DNA damage compared to that induced by transfer of exosomes collected at 24 hours post-irradiation. In addition, rapid calcium fluxes were induced in MEF recipient cells following addition of exosomes from brain, heart and liver from WBI and PBI mice but not from sham irradiated mice at 24 hours and 15 days post irradiation, as well as exosomes from plasma from WBI and PBI mice but not from sham irradiated mice at 24 hours post irradiation. Finally, transfer of exosomes from brain, heart and liver from mice 24 hours and 15 days after WBI or PBI and from plasma from mice 24 hours after WBI or PBI from caused significant ROS and NO production within 5 minutes from exosome addition.

Alltogether these data clearly demonstrated that exosomes may mediate radiation signaling by modifying viability and DNA damage in recipient cells, they provide a proof of principle of their role in mediating out-of-target radiation effects.

Task 3.3 In vivo exosome transfer, role of connexin43 (ENEA, OBU)

A further step in proving the involvement of exosomes in the propagation of radiation signaling is the in vivo functional testing. Exosomes derived from 2Gy-PBI or 2 Gy-WBI plasma/organs have been injected in the brain of non-irradiated recipient neonatal mice.

A preliminary pilot study was carried out at ENEA to test the labelling efficiency of PKH67 using the 3T3 fibroblast cell line. Cells were incubated for 24h with exosomes derived from organs collected 24 hours after RX and fluorescent microvesicles are shown in Fig 26.

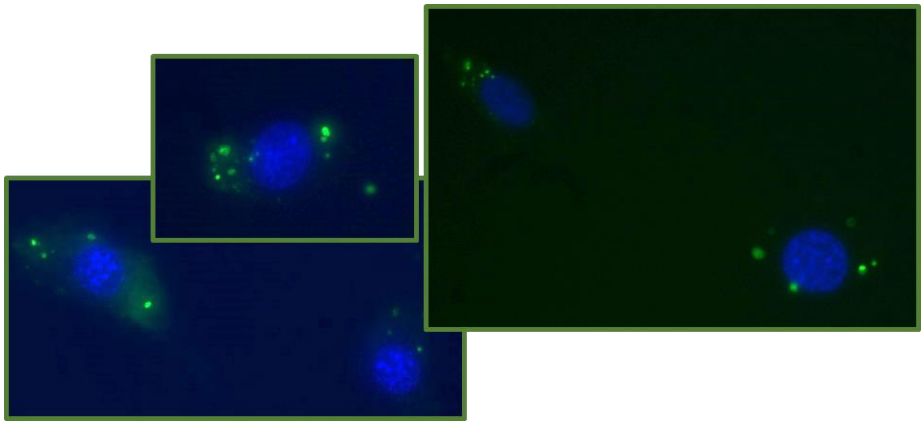

Fig. 26. PKH67 exosome labelling. PKH67 labelled exosomes were added to the 3T3 fibroblast cell line, and are visible in green.

Next we have intracranially injected about 1.2x109 PKH67 labelled exosomes in 5 □l of PBS in C57BL/6 mice at postanatal day 2 using a Hamilton syringe (Fig. 54). The injection site was located in the cerebellum area. Brains were OCT-embedded 30 min or 4h after injection for morphological analysis. Cerebella were also snap frozen (n=3 per each treatment). Fluorescent microvesicles are visible in green in the brain tissue (Fig. 27).

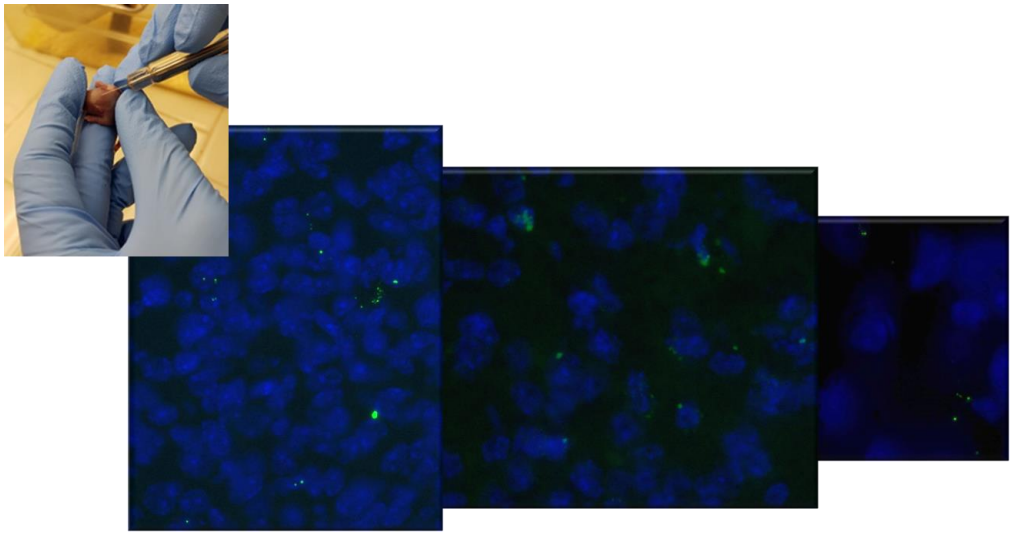

Fig.27. Intracranial injection of exoxome suspensions in the cerebellum of C57Bl6 mice at postnatal day 2. Fluorescent exosomes in green are detectable in the brain tissue.

The CD9 protein is one of the most ubiquitously expressed proteins on the exosomal surface and therefore considered an exosome marker. We further demonstrated the internalization of exosomes in the brain cells (Fig. 28).

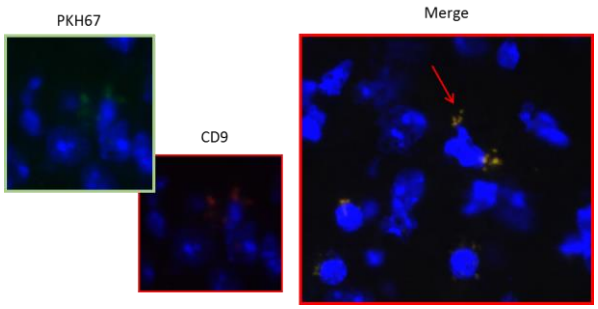

Fig. 28. Immunostaining with the exosome marker CD9.

To detect cellular damage in vivo we have performed a pilot experiment analysing cerebellar proteins through Western blot for cleaved-caspase-3, an apoptotic marker. We analyzed untreated cerebellum (0 Gy), sham-injected cerebellum (PBS), cerebellum injected with 0 Gy-plasma-derived exosomes (EXO 0 Gy), with 2 GyPBI-plasma-derived exosomes (EXO PBI), with 2 GyWBI-plasma-derived exosomes (EXO WBI) and cerebellum from 2 Gy whole body irradiated P2 mice. All the brains have been collected at 6 hours post treatment. We were able to show a robust caspase-3 response only in the whole body irradiated cerebellum but not in any of the EXO-injected brains (Fig. 29).

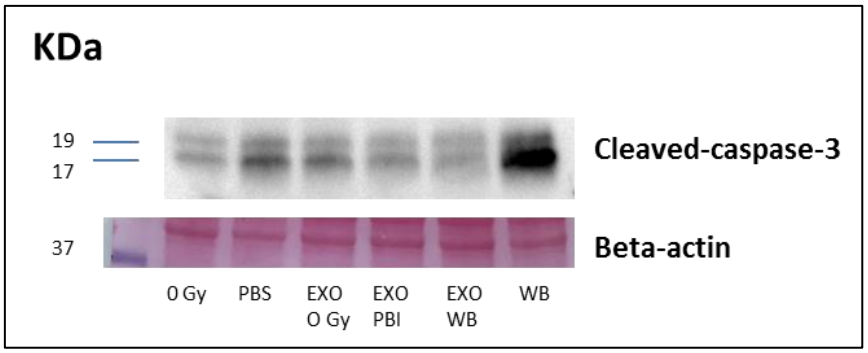

Fig. 29. Western blot analysis of total cerebellum proteins for Cleaved-caspase-3. Lane 1: size marker; lane 2 untreated cerebellum (0 Gy); lane 3 sham-injected cerebellum (PBS); lane 4: cerebellum injected with 0 Gy-plasma-derived exosomes (EXO 0 Gy); lane 5: cerebellum injected with 2 GyPBI-plasma-derived exosomes (EXO PBI); lane 6: cerebellum injected with 2 GyWBI-plasma-derived exosomes (EXO WBI), lane 7: cerebellum from 2 Gy whole body irradiated P2 mice. Below the corresponding β-actin levels for normalization.

The analysis of cerebella collected at shorter time after exosome injection (30 min) for □-H2AX, a DSBs marker is currently in progress. In addition, we will examine histological sections of cerebellum for the presence of apoptotic cells around the injection sites.

Task 3.4 Neuroinflammation (ENEA, OBU)

High-dose irradiation is often accompanied by neuroinflammation and chronic microglia activation. To investigate potential effects of out-of-target irradiation on microglia we have evaluated microglial cells labelled with ionized calcium-binding adapter molecule-1 (IBA1) in the hippocampus by immunohistochemistry in brain sections from PBI, WBI or unexposed mice at 15 days post-irradiation.

PBI irradiation, significantly increased IBA1 staining of 14.7% compared to unexposed mice (p = 0.0373) and there was a slight but non-significant increase in WBI versus control (Fig. 30).

Further experiments to characterize microglia response are still in progress, as well as the analysis with IBA1 in PBI and WBI brains at 6 months post-irradiation.

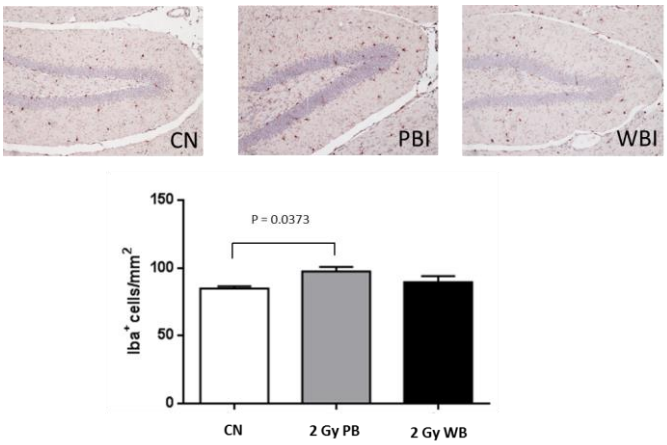

Fig. 30. Immunohistochemistry for the microglial marker IBA1 in the hippocampus of PBI, WBI or unexposed mice. The number of IBA1 positive cells per mm2 is plotted. Significant increase of IBA1 positive cells were in PBI samples at 15 days post-irradiation (p = 0.0373).

Summary and conclusions

The concept that radiation effects are not confined to directly irradiated tissues has been described in a wide variety of experimental systems (in vitro, cultured artificial 3-D human tissue systems, ex vivo models). In the attempt to fill the general lack of in vivo studies, in the last decade, research activities have been focused on in vivo validation of non-targeted effects, with the main emphasis on implications for cancer. Since non-cancer diseases, in particular neurocognitive, cardiovascular and metabolic liver disease, are common consequences of direct radiation exposure, the SEPARATE project investigated abscopal radiation effects on brain, heart, and liver following exposures that completely spare these organs. A multi-omic approach was applied to identify key mechanisms in out-of-target radiation effects. Changes in transcriptome, non-coding RNAs, protein and metabolic levels in these important organs provided a proof of principle of the out-of-target radiation response, especially in the hippocampus for which the investigations are at a more advanced stage. Similar changes in miRNAs and proteomic profiles were observed in the hippocampus after 2Gy-PBI and 2 Gy-WBI at 15 days post-irradiation. Proteomic-based bioinformatics analysis shows that biological pathways altered after WBI and PBI were associated with learning and memory. Accordingly, very similar defects in hippocampal neurogenesis were shown between WBI and PBI mice, mainly consisting in alterations of the stem cell compartment and self-renewal, pointing to a complex disturbance in the control of progression of neural stem cells into neurons. These defects disappeared with time (6 months) in PBI but not WBI hippocampus. Raman spectroscopy, that was not able to detect metabolic similarity in the hippocampus of 2 Gy-PBI and 2 Gy-WBI mice at 15 days post-irradiation, showed them at 6 months post-irradiation, indicating the progressive nature of the radiation-induced metabolic changes. Together, omics and cellular findings prove the existence of out-of-target radiation responses in the hippocampus in vivo.

We also investigated exosomes from exposed and shielded organs, and their specific bioactive cargo, for their potential role in mediating out-of-target effects in vitro and in vivo. Results show that irradiation increases the yield of exosomes derived from WBI and PBI organs at 24 hours and 15 days post-irradiation, without affecting their size distribution. Exosomes from WBI, PBI and unexposed

organs isolated at 24 hours post-irradiation were also analyzed in terms of proteome. Results showed that the cargo of exosomes from different organs (whole brain, liver, heart) reflects primarily the main components of the organ in question. In the brain, the exosomal proteins belong mainly to compartments only found in the brain such as myelin sheaths, synapses or axons. Changes in the miRNA cargo of plasma exosomes from 24 hours post WBI and PBI mice with 2 Gy of X-rays were also analyzed by NGS and compared with controls. All the differentially expressed miRNAs were up-regulated both in PBI and WB samples; however, a higher number of differentially expressed miRNAs were found after WBI (n= 57) compared with PBI (n=13), with only 5 miRNAs in common. Further investigations will be necessary to understand their possible role in mediating out-of-field effects.

Several relevant in vitro functional assays have been carried out in recipient MEF cells after incubation with exosomes from PBI and WBI mouse organs and plasma. Reduction of viability, increase of DNA damage, induction of rapid calcium fluxes and production of ROS and NO, are observed following addition of WBI and PBI exosomes to recipient MEFs. Highest γH2AX foci levels are observed in MEFs treated with both WBI and PBI brain exosomes isolated at 24 hours post-irradiation, while exosomes from plasma are more effective in inducing larger amount of DNA in comet tail and chromosome aberrations. Exosomes from 15 days post IR mouse organs also induces DNA damage, as shown with comet assays, but to a lesser extent compared to 24 hours post IR samples, as there was no significant increase of γH2AX foci levels or chromosomal aberrations.

A final ongoing step of the SEPARATE project is to establish the involvement of exosomes in the propagation of radiation signaling through in vivo functional assays. PKH67 labelled exosomes (1.2x109) derived from 2Gy-PBI or 2 Gy-WBI plasma/organs, were intracranially injected in the brain of non-irradiated recipient neonatal mice and their cell internalization was demonstrated by fluorescence microscopy. However, in this experimental condition, we were not able detect an apoptotic response of the exosomes-in the injected brains. Further experiments will be carried out within the end of the project modifying exosome concentrations and experimental time points.

In conclusion, the work performed within the project advanced the state of the art in the somewhat underdeveloped radiological area investigated, namely out-of-target radiation effects. Altogether these findings, obtained using a range of relevant experimental endpoints, provide a robust proof of principle of out of target radiation response in vivo and demonstrated that exosomes are able to propagate radiation signaling and modifying viability and DNA damage of recipient cells. However, further work is needed to identify the responsible mediator of the radiation-induced signals transmission. Importantly, the ongoing analysis of the bioactive exosomal cargo (both miRNAs and proteins) might add important information on this strategic aspect.

WP4 – Project Management

The SEPARATE consortium is made up of internationally recognized leaders from the relevant fields of radiation research. The combination of knowledge and skills provided scientific added value and excellent opportunity for integrative research. Moreover, the history of cooperative research among consortium members has mitigated risks associated with the project, meanwhile ensuring that the consortium could operate independently of other initiatives. No scientific, staff or collaborative difficulties are reported and there were no major deviations from the original work plan within the project period. The Advisory Board members have been an essential part of the SEPARATE throughout the lifetime of the project

WP5: Dissemination, training, exploitation

Publication

1. S. Pazzaglia, G. Briganti, M. Mancuso and A. Saran. Neurocognitive Decline Following Radiotherapy: Mechanisms and Therapeutic Implications. Cancers 2020, 12(1), 146. "Animal Models for Radiotherapy Research". Website online, DOI 10.3390/cancers12010146
2. M. Kadhim, A. Mayah, S. Brooks. Does direct and indirect exposure to ionising radiation influence metastatic potential of breast cancer cells? Cancers 2020, 12, 236; doi:10.3390/cancers12010236.

Communications in scientific congresses and conferences

1. F. Antonelli, P. Giardullo, S. Pazzaglia, B. Tanno, G. Babini, C. Merla, M. Khadim, F. Lyng, S. Tapio, A. Saran, M. Mancuso. Changes in neurogenesis and miRNA profiles in out-of field hippocampus from partial-body irradiated mice. European Radiation Protection Week 2019, Stockholm, Sweden 14-18 October 2019.
2. M. Mancuso. The SEPARATE project: origin and perspectives. ICRR 2019 Satellite meeting. Extracellular vesicles in mediating bystander and systemic RT effects. Manchester, August 25.
3. M. Kadhim, A. Mayah, S. Tuncay Cagatay, M. Mancuso, P. Giardullo, S. Pazzaglia, A. Saran, F. Lyng, S. Tapio. Exosome signalling roles in the non-targeted effects of radiation: investigating tissue and organ dependence. ICRR2019 Satellite meeting. Extracellular vesicles in mediating bystander and systemic RT effects. Manchester, August 25.
4. A. Mayah, S. Tuncay Cagatay, F. Lyng, S. Tapio, S. Pazzaglia, P. Giardullo, F. Antonelli, M. Mancuso, A. Saran, M. Kadhim. Characteristics of exosomes/MVs derived from different organs post in vivo Whole Body Irradiation (WBI) & Partial Body Irradiation (PBI). ICRR 2019: Parallel Session 3: Mitigation and Whole Body RT Effects, Manchester, August 25-29.
5. S. Tuncay Cagatay, A. Mayah, M.Mancuso, P. Giardullo, S. Pazzaglia, A. Saran, F. Lyng, S. Tapio, M. Kadhim. Non-targeted effects of exosome-mediated radiation signalling: comparison of whole and partial body irradiation. ICRR 2019: Poster , Manchester, August 25-29.
6. S. Pazzaglia, F. Antonelli, B. Tanno, P. Giardullo, G. Babini, C. Merla, M. Khadim, F. Lyng, S. Tapio, A. Saran, M. Mancuso. Out of field hippocampus from partial-body irradiated mice displays defects in neurogenesis and changes in miRNA profiles nearly identical to those induced by whole-body exposure. ICRR2019, Manchester 25-29 August.
7. D. Traynor, A. Daniel, M. Kadhim, S. Tapio, P. Giardullo, S. Pazzaglia, M. Mancuso, A. Saran, A. D. Meade, F. Lyng. Raman spectroscopic signatures in murine hippocampus following partial body irradiation. European Conference on Spectroscopy of Biological Molecules, Dublin, August 19-22, 2019.
8. A. Daniel, D. Traynor, S. Tuncay Cagatay, A. Mayah, M. Kadhim, S. Tapio, P.Giardullo, S. Pazzaglia, M. Mancuso, A. Saran, A. D. Meade, F. Lyng. Raman spectroscopic analysis of out of target effects mediated by exosomes from whole body and partial body irradiated mice. European Conference on Spectroscopy of Biological Molecules, Dublin, August 19-22, 2019.
9. S. Tuncay Cagatay, A. Mayah, M.Mancuso, P. Giardullo, S. Pazzaglia, A. Saran, F. Lyng, S. Tapio, M. Kadhim. Non-targeted effects of exosomes –mediated radiation signaling: comparison of whole and partial body irradiation. European Radiation Protection Week 2019, Stockholm, Sweden 14-18 October 2019
10. A.Mayah, S. Tuncay Cagatay, M. Mancuso, P. Giardullo, S. Pazzaglia, A. Saran, F. Lyng, S. Tapio, H. Du, S. Jassim, M. Kadhim. The role of exosomes in non-targeted effects of radiation in vivo: assessment with evaluation by machine learning. 65th Annual Radiation research Society Meeting. November 3-6, San Diego, CA, 2019.
11. S. Pazzaglia, F. Antonelli, B. Tanno, P. Giardullo, G. Babini, C. Merla, M. Khadim, F. Lyng, S.Tapio, A. Saran, M. Mancuso. Defects in neurogenesis and changes in miRNA profiles in out of field

hippocampus after partial-body irradiation of mice. 65th Annual Radiation research Society Meeting. November 3-6, San Diego, CA, 2019.
12. D. Traynor, A. Daniel, M. Kadhim, S. Tapio, P. Giardullo, S. Pazzaglia, M. Mancuso, A. Saran, A. D. Meade, F. Lyng. Biochemical signatures in murine hippocampus following partial body irradiation. European Radiation Protection Week 2019, Stockholm, Sweden 14-18 October 2019.
13. D. Traynor, A. Daniel, S. Tuncay Cagatay, A. Mayah, M. Kadhim, S. Tapio, P.Giardullo, S. Pazzaglia, M. Mancuso, A. Saran, A. D. Meade, F. Lyng. Exosome mediated radiation signalling from whole body and partial body irradiated mice. European Radiation Protection Week 2019, Stockholm, Sweden 14-18 October 2019.
14. Z. Nisar Khan, O. Azimzadeh, S. Mortl, F. Metzger, M. Kadhim, F. Lyng, S. Pazzaglia, M. Mancuso, A. Saran, S. Tapio. Radiation –regulated proteomic profiling of murine hippocampus to lowa radiation doses. ICRR2019, Manchester 25-29 August.
15. S. Tapio, Z. Nisar K., O. Azimzadeh, F. Metzger, M. Kadhim, F. Lyng, S. Pazzaglia, M. Mancuso, A. Saran. “Out-of-target” effects in the murine hippocampus after partial body irradiation, RAD7, Herzeg Novi, Montenegro, 10-14 June 2019.
16. Z. Nisar Khan, O. Azimzadeh, S.Moertl, F. Metzger, A. Saran, M. Kadhim, F. Lyng, S. Tapio. “SEPARATE”: Systemic effects of partial-body exposure to low radiation doses. European Radiation Protection Week 2018, Rovinj, Croatia, 1-5 October 2018.

Other

1. Satellite joint meeting SEPARATE-LEUTRACK at ICRR 2019: Extracellular vesicles in mediating bystander and systemic RT effects (CONCERT), Manchester, August 25.
2. M. Mancuso. Background and state of the art in the field of abscopal radiation effects: developing the SEPARATE project. CONCERT WP5 Stakeholder Workshop, September 2017.
3. AIR2 special issue edition February 2018
4. https://sites.google.com/view/separate-project/home